Spatiotemporal Features of Ca^{2+} Buffering and Diffusion in Atrial Cardiac Myocytes with Inhibited Sarcoplasmic Reticulum

Anushka Michailova,*† Franco DelPrincipe,* Marcel Egger,* and Ernst Niggli*
*Department of Physiology, University of Bern, Bern, Switzerland; and †Department of Biophysics, Bulgarian Academy of Science, Sofia, Bulgaria

ABSTRACT Ca^{2+} signaling in cells is largely governed by Ca^{2+} diffusion and Ca^{2+} binding to mobile and stationary Ca^{2+} buffers, including organelles. To examine Ca^{2+} signaling in cardiac atrial myocytes, a mathematical model of Ca^{2+} diffusion was developed which represents several subcellular compartments, including a subsarcolemmal space with restricted diffusion, a myofilament space, and the cytosol. The model was used to quantitatively simulate experimental Ca^{2+} signals in terms of amplitude, time course, and spatial features. For experimental reference data, L-type Ca^{2+} currents were recorded from atrial cells with the whole-cell voltage-clamp technique. Ca^{2+} signals were simultaneously imaged with the fluorescent Ca^{2+} indicator Fluo-3 and a laser-scanning confocal microscope. The simulations indicate that in atrial myocytes lacking T-tubules, Ca^{2+} movement from the cell membrane to the center of the cells relies strongly on the presence of mobile Ca^{2+} buffers, particularly when the sarcoplasmic reticulum is inhibited pharmacologically. Furthermore, during the influx of Ca^{2+} large and steep concentration gradients are predicted between the cytosol and the submicroscopically narrow subsarcolemmal space. In addition, the computations revealed that, despite its low Ca^{2+} affinity, ATP acts as a significant buffer and carrier for Ca^{2+}, even at the modest elevations of $[Ca^{2+}]_i$ reached during influx of Ca^{2+}.

GLOSSARY

Abbreviations

RSP	Restricted subsarcolemmal space;
MYOF	Myofibrillar space;
SR	Sarcoplasmic reticulum;
RyR	Ryanodine receptor;
DHPR	Dihydropyridine receptor (L-type Ca^{2+} channel);
ATP	Adenosine triphosphate.

Geometric parameters and constants

R	Cell radius;
L	Cell length;
C_m	Cell capacitance;
V_{cell}	Cell volume;
d_{RSP}	Restricted space thickness;
V_{rd}	Thin boundary volume between extracellular space and RSP;
rd	Boundary thickness;
V_{acc}	Accessible volume for Ca^{2+} in the cell;
S	Model cell surface through which Ca^{2+} enters.

Concentrations and reaction parameters

$[Ca^{2+}]_i$	Free intracellular Ca^{2+} concentration;
$[Ca^{2+}]_o$	Extracellular Ca^{2+} concentration;
$[Ca^{2+}]_{rest}$	Resting Ca^{2+} concentration;
[TN]	Total troponin concentration (low-affinity sites);
[CAL]	Total calmodulin concentration;
[PL]	Total phospholipid concentration (low-affinity sites);
[PH]	Total phospholipid concentration (high-affinity sites);
[FLUO]	Total Fluo-3 concentration;
[ATP]	Free ATP concentration;
[CaTN]	Ca^{2+}-troponin concentration (low-affinity sites);
[CaCAL]	Ca^{2+}-calmodulin concentration;
[CaPL]	Ca^{2+}-phospholipid concentration (low-affinity sites);
[CaPH]	Ca^{2+}-phospholipid concentration (high-affinity sites);
[CaFLUO]	Ca^{2+}-Fluo-3 concentration;
[CaATP]	Ca^{2+}-ATP concentration;
D_{RSP}^{Ca}	Diffusion coefficient for Ca^{2+} in RSP;
D_{MYOF}^{Ca}	Diffusion coefficient for Ca^{2+} in MYOF;
D_{RSP}^{CaCAL}	Diffusion coefficient for CaCAL in RSP;
D_{MYOF}^{CaCAL}	Diffusion coefficient for CaCAL in MYOF;
D_{RSP}^{CaFLUO}	Diffusion coefficient for CaFLUO in RSP;
D_{MYOF}^{CaFLUO}	Diffusion coefficient for CaFLUO in MYOF;
D_{MYOF}^{CaATP}	Diffusion coefficient for CaATP in MYOF;
D_{RSP}^{CaATP}	Diffusion coefficient for CaATP in RSP;

Submitted May 17, 2001, and accepted for publication July 19, 2002.

Address reprint requests to Dr. Ernst Niggli, Dept. of Physiology, University of Bern, Buehlplatz 5, CH-3012 Bern, Switzerland.

A. Michailova's present address is Dept. of Bioengineering, University of California, San Diego, La Jolla, CA. Tel.: +41-31-631-8730; Fax: +41-31-631-4611; E-mail: niggli@pyl.unibe.ch.

0006-3495/02/12/3134/18 $2.00

k_+^{TN} Ca^{2+} on-rate constant for troponin (low-affinity sites);
k_-^{TN} Ca^{2+} off-rate constant for troponin (low-affinity sites);
k_+^{CAL} Ca^{2+} on-rate constant for calmodulin;
k_-^{CAL} Ca^{2+} on-rate constant for calmodulin;
k_+^{PL} Ca^{2+} off-rate constant for phospholipid (low-affinity sites);
k_-^{PL} Ca^{2+} off-rate constant for phospholipid (low-affinity sites);
k_+^{PH} Ca^{2+} on-rate constant for phospholipid (high-affinity sites);
k_-^{PH} Ca^{2+} off-rate constant for phospholipid (high-affinity sites);
k_+^{FLUO} Ca^{2+} on-rate constant for Fluo-3;
k_-^{FLUO} Ca^{2+} off-rate constant for Fluo-3;
k_+^{ATP} Ca^{2+} on-rate constant for ATP;
k_-^{ATP} Ca^{2+} off-rate constant for ATP;
$J_{I_{Ca}}$ Ca^{2+} flux via L-type Ca^{2+} channels;
F Faraday's constant;
I_{Ca} L-type Ca^{2+} current;
I_0 Constant;
a_i, b_j Constants;
J_{exch} Ca^{2+} flux through Na^+/Ca^{2+} exchanger;
$V_{max,x}$ Maximal velocity of Na^+/Ca^{2+} exchanger;
K_m Ca^{2+} concentration at half $V_{max,x}$;
n Hill's coefficient;
J_{exl} Inward Ca^{2+} leak flux via plasma membrane;
L_m Ca^{2+} leak constant.

INTRODUCTION

In cardiac and skeletal muscle cells mechanical activity is controlled by a transient elevation of the intracellular Ca^{2+} concentration ($[Ca^{2+}]_i$) (Taylor et al., 1975; Cannell et al., 1987; Niggli, 1999). Compared to other cell types, striated muscle cells are quite large. Depending on the diameter of a given muscle cell, diffusion of Ca^{2+} from the cell membrane to the proteins regulating muscle force (i.e., troponin C) would introduce unacceptable delays in the activation of contraction. Reasons for this delay are the sheer distance and the presence of stationary Ca^{2+} buffers in the cell, which tend to slow the movement of Ca^{2+} (Crank, 1975; Neher and Augustine, 1992; Jafri and Keizer, 1995; Haddock et al., 1999). Therefore, several structural and functional systems have evolved to accelerate the spread of Ca^{2+} signals in muscle cells considerably. Skeletal and most cardiac muscle cells have developed deep invaginations of the extracellular space via infoldings of the cell membrane. These so-called T-tubules form a network of extracellular space, extending deep into the cell interior and allowing the fast electrical signal (i.e., the action potential) to be carried close to the subcellular location where Ca^{2+} is needed (Bers, 2001). In addition, intracellular Ca^{2+} stores are present in most species (i.e., the sarcoplasmic reticulum (SR)). In cardiac muscle Ca^{2+} release from these stores drastically reduces the amount of Ca^{2+} that has to enter from the extracellular space, while in skeletal muscle it represents the almost exclusive source of Ca^{2+}. Besides acting as an amplifier of the trigger signals, Ca^{2+} release from the SR also acts as an accelerator for the spatial spread of Ca^{2+} signals (Dawson et al., 1999). In skeletal muscle, Ca^{2+} release from the SR initially occurs via Ca^{2+} release channels (ryanodine receptors; RyRs) that are under the control of voltage sensors located in the sarcolemma (Schneider and Chandler, 1973; Rios et al., 1991). In cardiac muscle, the RyRs are controlled by the Ca^{2+}-induced Ca^{2+} release mechanism (CICR; Fabiato, 1983). The trigger Ca^{2+} is provided by influx via L-type Ca^{2+} channels (DHP receptors), which represent the structural and functional equivalent of the voltage sensors present in skeletal muscle. By working together, the T-tubules and the Ca^{2+} release from the SR ensure spatially homogeneous and synchronized Ca^{2+} release throughout each cell.

In many species atrial cardiac muscle cells have no T-tubules and are thus an interesting exception to the rule (Bers, 2001). Although generally exhibiting smaller diameters than ventricular myocytes, these cells might encounter Ca^{2+} diffusion delays if SR Ca^{2+} release from the SR fails (Lipp et al., 1990; Hüser et al., 1996; Kockskämper et al., 2001). They may have developed a dense network of Ca^{2+} stores close to the sarcolemma, but also deep inside the cell, to compensate partly for the lack of T-tubules. In the absence of functional T-tubules, Ca^{2+} signals are known to spread rapidly from one SR Ca^{2+} release site to the next, giving rise to saltatoric reaction-diffusion waves (Hüser et al., 1996; Cheng et al., 1996; Keizer and Smith, 1998; Kockskämper et al., 2001).

In the present study we examined Ca^{2+} diffusion in atrial cells that had been treated with ryanodine and thapsigargin to eliminate release and uptake of Ca^{2+} by the SR. Using a combination of experimental techniques and a mathematical model, we could analyze several important spatial and temporal features of Ca^{2+} diffusion and signaling in these cells. In this context, the goal was at least threefold. The first aim was to develop a mathematical model that would quantitatively predict our experimental results on Ca^{2+} influx, Ca^{2+} buffering, and Ca^{2+} diffusion in atrial cells, when the SR was inhibited. Second, we used the model to explore the parameter space beyond the experimentally accessible limits. The third task was to use the model to examine the importance of mobile and stationary Ca^{2+} buffers and the effect of altered restricted space geometry for the Ca^{2+} signals. The restricted space is also known as the "fuzzy space" (Lederer et al., 1990) and is below the optical

resolution of confocal (optical) microscopes. Inclusion of the fuzzy space was not required to model the experimental results, but allowed explorations and predictions of Ca^{2+} signals in this space. Furthermore, our model calculations suggest an important role for mobile and stationary Ca^{2+} buffers, including the Ca^{2+} indicator dye used in our experiments. The model also predicts a significant acceleration of Ca^{2+} diffusion by physiological concentrations of the low-affinity Ca^{2+} buffer ATP. Preliminary results of this work have been presented to the Biophysical Society in abstract form (Michailova et al., 1999).

MATERIALS AND METHODS

Cell isolation and solutions

Experiments were performed on single atrial myocytes isolated enzymatically from guinea pigs (*Cavia porcellus*). The isolation procedure used was a modification of the method reported by Kockskämper and Glitsch (1997). Adult animals were killed by cervical dislocation, the hearts rapidly removed, and retrogradely perfused for 3 min on a Langendorff perfusion system at 37°C. The perfusing solution consisted of basic Ca^{2+}-free solution (in mM: sucrose 204, NaCl 35, KCl 5.4, $MgCl_2$ 1, HEPES 10, pH 7.4 adjusted with NaOH) with 2 mM ethylene glycol-bis-(β-aminoethylether)-*N*,*N*,*N*′,*N*′-tetraacetic acid (EGTA). Enzymatic digestion was started by switching to Ca^{2+}-free solution containing collagenase B (0.2 mg/ml; Boehringer Mannheim, Rotkreuz, Switzerland), protease type XIV (0.05 mg/ml; Sigma, Buchs, Switzerland) and elastase (5 μl/ml; Serva, Heidelberg, Germany). To promote the digestion of the atria the large blood vessels were ligated and the heart was immersed in an organ bath.

After 15 min the atria were minced, placed in Ca^{2+}-free solution containing 1 mg/ml bovine serum albumin (BSA) to stop the digestion, and left on a rocking table at room temperature (22°C) to allow for dispersion of the tissue. During this procedure (~1-h) the cells were adapted to calcium by dropwise addition of an equal volume of cell culture medium containing 1.26 mM Ca^{2+} (M199, Gibco, Basel, Switzerland) and supplemented with 100 IU/ml penicillin, 100 μg/ml streptomycin, and 10% fetal calf serum (all from Gibco). Finally, cells were taken from the supernatant and plated onto glass coverslips placed in culture dishes. The cells were incubated overnight at 37°C and 5% CO_2 and used the following day.

Current measurements

All experiments were carried out at room temperature (22°C). A coverslip with adherent cells was assembled into a recording chamber and mounted onto the stage of an inverted microscope (Diaphot TMD, Nikon, Küsnacht, Switzerland). The cells were constantly superfused (1–2 ml/min) with extracellular solution containing (in mM) NaCl 140, KCl 5, $MgCl_2$ 1, $CaCl_2$ 1, glucose 10, HEPES 10, pH 7.4 adjusted with NaOH. Patch-clamp recording electrodes were pulled from filamented borosilicate glass capillaries (GC150F, Clark Electromedical Instruments, Pangbourne, UK) on a horizontal puller (DMZ, Zeitz Instruments, Augsburg, Germany) and filled with intracellular solution containing (in mM): CsAsp 120, NaCl 10, TEA-Cl 20, HEPES 20, MgATP 5, $MgCl_2$ 1, Fluo-3 0.1, pH 7.2 adjusted with CsOH. The free $[Ca^{2+}]$ calculated for this solution was 99 nM (when assuming a typical Ca^{2+} contamination of 15 μM). Pipette resistances ranged from 2 to 4 MOhm. Cells were voltage-clamped in the whole-cell configuration and held at −70 mV without correction for the liquid junction potential (Axopatch 200, Axon Instruments, Foster City, CA). The voltage was stepped to −40 mV for 50 ms to inactivate the Na^+ current and subsequently to 0 mV for 200 ms to elicit a Ca^{2+} current. The step to −40 mV was introduced to avoid any residual Na^+ current that would contaminate the recording of the Ca^{2+} current despite the presence of 10 μM tetrodotoxin (TTX). In addition, the Ca^{2+} current was enhanced by application of 1 μM isoproterenol.

Series resistance and membrane capacitance were compensated with the built-in compensation circuit of the amplifier. The reading on the capacitance compensation dial of the amplifier was taken as the membrane capacitance of the cell. No leak subtraction was performed. The pure Ca^{2+} current was determined off-line by subtracting the current recorded in the presence of 5 mM Cd^{2+}. Currents were low-pass filtered at 5 kHz and digitized at 10 kHz using the LabView data acquisition software (National Instruments, Ennetbaden, Switzerland). Data were stored on hard disk for later analysis with the IgorPro software (WaveMetrics, Lake Oswego, OR).

Thapsigargin and TTX were purchased from Alomone Labs (Jerusalem, Israel), ryanodine from Calbiochem (La Jolla, CA), isoproterenol from Fluka (Buchs, Switzerland), and Fluo-3 (penta-potassium) from TefLabs (Austin, TX). Cells were incubated with thapsigargin and ryanodine for 30 min before each experiment to block the SR Ca^{2+} pump and the ryanodine receptor. Thapsigargin was dissolved as 1 mM stock in ethanol and used at 0.1 μM. Ryanodine was dissolved at 10 mM in distilled water and used at 10 μM concentration. Isoproterenol stock solution (10 mM) was freshly prepared before each experiment in distilled water containing 1 mM L-ascorbic acid and added at 1 μM to the extracellular solution. TTX was dissolved in distilled water, kept in aliquots at −20°C as a stock solution (10 mM) and used at 10 μM. Fluo-3 was reconstituted in distilled water to 5 mM and diluted to 0.1 mM into the pipette filling solution. Drugs were delivered to the cells through a gravity-driven rapid superfusion system.

Confocal Ca^{2+} measurements

Cells were viewed with a 40× oil-immersion objective (Fluor, N.A. = 1.3, Nikon) and loaded with Fluo-3 through the recording pipette. Fluo-3 was excited with the 488 nm line of an argon laser (model 5000, Ion Laser Technology, Salt Lake City, UT) at 50 μW intensity on the cell. The fluorescence was detected at 540 ± 15 nm with a photomultiplier tube (PMT) of a laser-scanning confocal system (MRC 1000, Bio-Rad, Glattbrugg, Switzerland) operated in the line-scan mode. The recording chamber was rotated to position the cell's width in parallel to the scan direction. The scan speed was set to 2 ms per line. Synchronization of the Ca^{2+} signal with the voltage protocol was assured by simultaneously recording a red light-emitting diode, triggered by the acquisition software, with the second PMT of the confocal system (>600 nm).

To record the Ca^{2+} influx generated by the activation of L-type Ca^{2+} channels without contamination by CICR from the SR, the cells were treated with 10 μM ryanodine and 0.1 μM thapsigargin. Amplitude and time course of Ca^{2+} signals due to Ca^{2+} influx were computed off-line using a customized version of the NIH Image software (NIH, Bethesda, MD). Different regions of interest (width = 1–2 μm) were chosen to average the temporal Ca^{2+} concentration changes near the plasmalemma or in the center of the cell. Similarly, Ca^{2+} concentration profiles across the entire width of the cell were extracted for each time point (2 ms). The spatial profiles of $[Ca^{2+}]_i$ are limited by optical diffraction, while the mathematical simulation can exhibit a much better spatial resolution. The point-spread-function of our confocal microscope was examined with fluorescent beads (diameter 100 nm) and was determined to have a full-width at half-maximal amplitude (FWHM) of 350 nm · 350 nm · 900 nm (for the *x*, *y*, and *z* dimension, respectively). Ca^{2+} concentration was calculated from fluorescence images using an established self-ratio calibration procedure (Cheng et al., 1993). For the calibration we assumed a K_d value for Fluo-3 of 739 nM and a resting Ca^{2+} concentration of 100 nM at the beginning of each experiment. Surface plots were generated from

line-scan images using the IDL software (Research Systems, Boulder, CO). Confocal *x-y* images were used to calculate the surface and the volume of the cells using the NIH Image software. The accuracy of the procedure was verified by comparing the results with the values obtained using the measured membrane capacitance (assuming 1 μF capacitance per cm^2 of membrane).

Mathematical model

We developed a mathematical model of Ca^{2+}-signaling, Ca^{2+}-diffusion, and Ca^{2+}-buffering inside an atrial cardiac muscle cell. The goal was to simulate and analyze Ca^{2+} events, which were recorded on the confocal microscope and, in addition, to simulate Ca^{2+} signals that are not accessible experimentally. In view of the fact that the isolated atrial myocyte has an approximately cylindrical shape (see Fig. 1 *A*) and lacks T-tubules (Bers, 2001; Hüser et al., 1996; Kockskämper et al., 2001) a cylindrical geometry is assumed (see Fig. 2 *A*).

Model cell geometry

The model cell geometry was derived from the experimental data. The guinea pig atrial myocyte used for this study had a spindle shape (see Fig. 1 *A*) with a maximal diameter of 15.6 μm, a cell length of 125 μm, and a membrane capacitance of 41 pF. For the model, the shape was simplified into a cylinder that had the same diameter (see Fig. 2 *A*). The actual cylinder length was decreased from 125 μm to 83.7 μm to adjust the volume accessible for Ca^{2+} (~50%, see below) to be consistent with that of the real atrial myocyte. It is necessary to note that scaling of the cell length is allowed because the model simulates the radial diffusion only. Therefore, other accessible volume fractions were simulated by changing the length of the cylinder and by scaling the densities of the membrane currents accordingly.

The accessible volume for Ca^{2+} was estimated on the basis of the data by Forbes and Van Niel (1988) in guinea pig atrium (see also Bers, 2001 and Table 1). In accordance with these data the myofilaments occupy 43.2% of the cell volume, mitochondria 17.9%, the nucleus 3.8%, T-tubule 0.08%, and SR 9.93%. For simplification we assumed that the volume occupied by T-tubules is zero, as several reports indicate that guinea pig atrial muscle cells have no T-tubules (Bers, 2001; Hüser et al., 1996). The experimental data also suggest that ~50% of the myofilament space is accessible for Ca^{2+} ions (i.e., contains water) and that mitochondria and nuclei are not rapidly accessible for Ca^{2+} (Bers, 2001). We also assume that the SR lumen is not accessible for Ca^{2+} in the presence of ryanodine and thapsigargin. Thus, in accordance with Forbes and Van Niel (1988) and above assumptions, the accessible volume for Ca^{2+} in guinea pig atrial cells was estimated to be ~50% of the total cytosolic volume (V_{acc} = 46.8% = 100% − 21.6% − 17.9% − 3.8% − 9.93%).

The model cell has two separate spaces, the restricted subsarcolemmal space (RSP) and the myofibrillar space (MYOF) (see Fig. 2 *A*). Ca^{2+} and mobile buffers, Fluo-3 and calmodulin, diffuse throughout the myocyte purely in the radial (r) direction and reflect from the cell walls.

Restricted subsarcolemmal space

In the literature, the restricted space (RSP) thickness (i.e., the distance between the SR and sarcolemmal membrane) is reported to be between 12 and 20 nm (Fawcett and McNutt, 1969; Forbes and Sperelakis, 1982; Langer and Peskoff, 1996; Soeller and Cannell, 1997). In our study, the width of this space was assumed to be 20 nm. Within the RSP Ca^{2+} ions are free to diffuse and react with the stationary Ca^{2+} buffers (phospholipids) and with the mobile Ca^{2+} buffers (calmodulin and Fluo-3). In the fuzzy space, the diffusion coefficients for Ca^{2+} and mobile buffers in the r-direction are assumed to be those in water (see Table 1). The one-dimensional diffusion equations for Ca^{2+}, calmodulin, Fluo-3, and phospholipids in the restricted subsarcolemmal space can be written in cylindrical coordinates as (for definitions, symbols, and abbreviations, please see "Glossary").

$$\begin{aligned}\frac{\partial[Ca^{2+}]_i}{\partial t} = {} & D_{RSP}^{Ca}\frac{1}{r}\frac{\partial}{\partial r}\left(r\frac{\partial[Ca^{2+}]_i}{\partial r}\right) + J_{I_{Ca}} - J_{exch} + J_{exl} \\ & - k_+^{FLUO}([FLUO] - [CaFLUO])[Ca^{2+}]_i \\ & + k_-^{FLUO}[CaFLUO] \\ & - k_+^{CAL}([CAL] - [CaCAL])[Ca^{2+}]_i \\ & + k_-^{CAL}[CaCAL] \\ & - k_+^{PL}([PL] - [CaPL])[Ca^{2+}]_i \\ & + k_-^{PL}[CaPL] \\ & - k_+^{PH}([PH] - [CaPH])[Ca^{2+}]_i \\ & + k_-^{PH}[CaPH] \end{aligned} \quad (1)$$

$$\begin{aligned}\frac{\partial[CaCAL]}{\partial t} = {} & D_{RSP}^{CaCAL}\frac{1}{r}\frac{\partial}{\partial r}\left(r\frac{\partial[CaCAL]}{\partial r}\right) \\ & + k_+^{CAL}([CAL] - [CaCAL])[Ca^{2+}]_i \\ & - k_-^{CAL}[CaCAL] \end{aligned} \quad (2)$$

$$\begin{aligned}\frac{\partial[CaFLUO]}{\partial t} = {} & D_{RSP}^{CaFLUO}\frac{1}{r}\frac{\partial}{\partial r}\left(r\frac{\partial[CaFLUO]}{\partial r}\right) \\ & + k_+^{FLUO}([FLUO] - [CaFLUO])[Ca^{2+}]_i \\ & - k_-^{FLUO}[CaFLUO] \end{aligned} \quad (3)$$

$$\frac{\partial[CaPL]}{\partial t} = k_+^{PL}([PL] - [CaPL])[Ca^{2+}]_i - k_-^{PL}[CaPL] \quad (4)$$

$$\frac{\partial[CaPH]}{\partial t} = k_+^{PH}([PH] - [CaPH])[Ca^{2+}]_i - k_-^{PH}[CaPH] \quad (5)$$

The Ca^{2+} flux via L-type Ca^{2+} channels ($J_{I_{Ca}}$) is proportional to the L-type Ca^{2+} current (I_{Ca}) recorded with the whole-cell voltage-clamp technique, Eq. 6.

$$J_{I_{Ca}} = \left(\frac{S}{2FV_{rd}}\right)I_{Ca} \quad (6)$$

The time course of $I_{Ca}(t)$ in Eq. 6 is approximated by the following equations:

$$I_{Ca}(t) = I_0 f(t) \quad (7)$$

where

$$\begin{aligned} f(t) &= a_1 + a_2\exp(-a_3 t) \quad t \le 0.02s \\ f(t) &= b_0 + b_1\exp(-b_2 t) + b_3\exp(-b_4 t) \quad t > 0.02s \end{aligned} \quad (8)$$

In the model the Hill equation is used to describe Ca^{2+} movement by the Na^+/Ca^{2+} exchanger (J_{exch}) (Cannell and Allen, 1984; Kargacin and Fay, 1991):

$$J_{exch} = \frac{V_{max,x}[Ca^{2+}]_i^n}{(K_m^n + [Ca^{2+}]_i^n)} \quad (9)$$

The inward Ca^{2+} leak flux through the plasma membrane (J_{exl}) is described by:

$$J_{exl} = L_m([Ca^{2+}]_o - [Ca^{2+}]_i) \quad (10)$$

Myofibrillar space

In the MYOF Ca^{2+} ions diffuse and react with stationary (troponin C) and mobile Ca^{2+} buffers (calmodulin and Fluo-3). In the myofibrillar space we assume that the diffusion coefficients for the free Ca^{2+} and mobile buffers are reduced in the *r*-direction because of the impediment imposed by myofilaments, mitochondria, SR, and other structures (i.e., structural tortuosity, see Table 1). Accordingly, the diffusion coefficients in the *r*-direction for the free Ca^{2+}, Fluo-3, and calmodulin in the MYOF and the RSP have different values because the MYOF and the RSP are morphologically different. The one-dimensional diffusion equations for Ca^{2+}, calmodulin, Fluo-3, and troponin C in the myofibrillar space can be written in cylindrical coordinates as:

$$\begin{aligned}\frac{\partial[Ca^{2+}]_i}{\partial t} = {} & D_{MYOF}^{Ca}\frac{1}{r}\frac{\partial}{\partial r}\left(r\frac{\partial[Ca^{2+}]_i}{\partial r}\right) \\ & - k_+^{FLUO}([FLUO] - [CaFLUO])[Ca^{2+}]_i \\ & + k_-^{FLUO}[CaFLUO] \\ & - k_+^{CAL}([CAL] - [CaCAL])[Ca^{2+}]_i \\ & + k_-^{CAL}[CaCAL] \\ & - k_+^{TN}([TN] - [CaTN])[Ca^{2+}]_i \\ & + k_-^{TN}[CaTN] \end{aligned} \quad (11)$$

$$\begin{aligned}\frac{\partial[CaCAL]}{\partial t} = {} & D_{MYOF}^{CaCAL}\frac{1}{r}\frac{\partial}{\partial r}\left(r\frac{\partial[CaCAL]}{\partial r}\right) \\ & + k_+^{CAL}([CAL] - [CaCAL])[Ca^{2+}]_i \\ & - k_-^{CAL}[CaCAL] \end{aligned} \quad (12)$$

$$\begin{aligned}\frac{\partial[CaFLUO]}{\partial t} = {} & D_{MYOF}^{CaFLUO}\frac{1}{r}\frac{\partial}{\partial r}\left(r\frac{\partial[CaFLUO]}{\partial r}\right) \\ & + k_+^{FLUO}([FLUO] - [CaFLUO])\cdot[Ca^{2+}]_i \\ & - k_-^{FLUO}[CaFLUO] \end{aligned} \quad (13)$$

$$\frac{\partial[CaTN]}{\partial t} = k_+^{TN}([TN] - [CaTN])[Ca^{2+}]_i - k_-^{TN}[CaTN] \quad (14)$$

In the model we also assume 1) Ca^{2+} binds to Fluo-3, calmodulin, troponin C, and phospholipids without cooperativity; 2) the initial total concentrations of the mobile buffers (Fluo-3 or calmodulin) are spatially uniform; and 3) the diffusion coefficients of Fluo-3 or calmodulin with bound Ca^{2+} are equal to the diffusion coefficients of free Fluo-3 or calmodulin.

Ca^{2+} current, Na^+/Ca^{2+} exchanger, and Ca^{2+} leak

To assess the influx of Ca^{2+} during cell excitation, the Ca^{2+} current was recorded with the whole-cell voltage-clamp technique. For the quantitative model, the simulated Ca^{2+} current was adjusted to match the experimentally acquired Ca^{2+} current record (Eqs. 7 and 8, Table 1).

The Na^+/Ca^{2+} exchanger and Ca^{2+} leak parameters were estimated or taken from the literature. Based on measurements of Na^+/Ca^{2+} exchange currents in atrial myocytes, we estimated the maximum exchanger velocity ($V_{max,x}$) at −70 mV to be ~853 $\mu M\ s^{-1}$ and ~85.3 $\mu M\ s^{-1}$ at 0 mV. In ventricular cells Backx et al. (1989) reported a $V_{max,x}$ of 1000 $\mu M\ s^{-1}$. The Ca^{2+} concentration at half $V_{max,x}$ (K_m) and the Hill coefficient (n) used during the simulations were those reported by Backx et al. (1989). The Ca^{2+} leak constant (L_m) was adjusted so that at rest the Na^+/Ca^{2+} exchanger efflux balanced the inward Ca^{2+} leak flux through the plasma membrane (Egger and Niggli, 1999).

Initial Ca^{2+} and buffer concentrations and buffer rate and dissociation constants

In the cytosolic space, basal Ca^{2+} concentration ($[Ca^{2+}]_{rest}$) is estimated to be 100 nM (Fabiato, 1983; Carafoli, 1985; Bers, 2001). It was found that the cells are able to maintain this Ca^{2+} level despite addition of exogenous dyes and buffers (Neher and Augustine, 1992). In this study, each simulation started with a resting Ca^{2+} concentration of 100 nM and buffers in equilibrium. The extracellular Ca^{2+} concentration ($[Ca^{2+}]_o$) was 1 mM and remained constant.

A number of powerful buffering systems for intracellular Ca^{2+} (SR, mitochondria, different stationary and mobile Ca^{2+} buffers) are known in cardiac muscle cells (Fabiato, 1983; Bers, 2001). As already mentioned, our model did not incorporate Ca^{2+} storing organelles, such as the SR and mitochondria; but because other stationary Ca^{2+} buffers (troponin C and phospholipids) and mobile Ca^{2+} buffers (calmodulin, Fluo-3, and ATP) strongly affect the Ca^{2+} dynamics in cardiac myocytes, these buffers were included in our model (Robertson et al., 1981; Fabiato, 1983; Bers, 2001; Harkins et al., 1993; Langer and Peskoff, 1996; Soeller and Cannell, 1997; Baylor and Hollingworth, 1998). Stationary Ca^{2+} buffers like troponin C and phospholipids are localized to different cell regions, while the mobile buffers diffuse throughout the entire cell.

Two classes of Ca^{2+} binding sites have been identified on cardiac troponin: low-affinity (Ca^{2+}-specific) and high-affinity (Ca^{2+}-Mg^{2+}) binding sites (Robertson et al., 1981). The high-affinity sites (K_d = 3.3 nM) are already saturated at resting $[Ca^{2+}]_i$. Therefore, only the Ca^{2+}-specific sites were included because large and rapid changes in the Ca^{2+} occupancy of these sites can occur during a Ca^{2+} transient (Robertson et al., 1981; Fabiato, 1983; Bers, 2001; Soeller and Cannell, 1997). We assumed that these binding sites are immobile because of their attachment to the actin filaments. The concentration of the Ca^{2+}-specific troponin sites is estimated to be 70 μM (published concentrations 50–150 μM for 50% accessible volume; Robertson et al., 1981; Fabiato, 1983). The dissociation constant (K_D^{TN} = 0.5 μM) and Ca^{2+} on- and off-rate constants were taken from Robertson et al. (1981).

Stationary low- and high-affinity Ca^{2+} binding sites on phospholipids were also included in our analysis because a major effect of these anionic sites on the time course of Ca^{2+} movements in the fuzzy space has been suggested (Langer and Peskoff, 1996; Soeller and Cannell, 1997; Peskoff and Langer, 1998). In agreement with the experimental observations, the phospholipid stationary sites were located on the inner sarcolemmal leaflet of our model cell (Post and Langer, 1992). The initial concentrations of the phospholipid sites and their affinities were taken from Peskoff and Langer (1998) (Table 1). Because we did not find any published data for the

TABLE 1 Cell geometry parameters

Definition	Symbol	Value	Source
Cell radius	R	7.8 μm	Experiment
Cell length	L	83.7 μm	Estimated
Cell capacitance	C_m	41 pF	Experiment
Cell volume	V_{cell}	15990 μm^3	Estimated
Restricted space thickness	d_{RSP}	0.02 μm	Soeller and Cannell, 1997
Boundary thickness	rd	0.003 μm	Estimated
Accessible volume for Ca^{2+} in the cell	V_{acc}	7483 μm^3	Estimated
Model cell surface	S	4100 μm^2	Estimated
Ca^{2+} and buffer concentrations			
Extracellular Ca^{2+} concentration	$[Ca^{2+}]_o$	1000 μM	Experiment
Resting Ca^{2+} concentration	$[Ca^{2+}]_{rest}$	0.1 μM	Bers, 2001
Total troponin concentration (low-affinity sites)	[TN]	70 μM	56–150 μM; Fabiato, 1983; Robertson et al., 1981
Total calmodulin concentration	[CAL]	24 μM	Fabiato, 1983
Total phospholipid concentration (low-affinity sites)	[PL]	165×10^3 μM	Peskoff and Langer, 1998
Total phospholipid concentration (high-affinity sites)	[PH]	13×10^3 μM	Peskoff and Langer, 1998
Total Fluo-3 concentration	[FLUO]	100 μM	Experiment
Free ATP concentration*	[ATP]	260 μM	Experiment
Diffusion coefficients			
Diffusion coefficient for Ca^{2+} in RSP	D_{RSP}^{Ca}	780 μm^2 s^{-1}	Kushmerick and Podolsky, 1969
Diffusion coefficient for Ca^{2+} in MYOF	D_{MYOF}^{Ca}	390 μm^2 s^{-1}	Kargacin and Fay, 1991
Diffusion coefficient for CaCAL in RSP	D_{RSP}^{CaCAL}	50 μm^2 s^{-1}	Simulation
Diffusion coefficient for CaCAL in MYOF	D_{MYOF}^{CaCAL}	25 μm^2 s^{-1}	Gabso et al., 1997
Diffusion coefficient for CaFLUO in RSP	D_{RSP}^{CaFLUO}	200 μm^2 s^{-1}	Simulation
Diffusion coefficient for CaFLUO in MYOF	D_{MYOF}^{CaFLUO}	100 μm^2 s^{-1}	Simulation
Diffusion coefficient for CaATP in RSP*	D_{RSP}^{CaATP}	320 μm^2 s^{-1}	Simulation
Diffusion coefficient for CaATP in MYOF*	D_{MYOF}^{CaATP}	168 μm^2 s^{-1}	Baylor and Hollingworth, 1998
Rate and dissociation constants (at 22°C)			
Ca^{2+} on-rate constant (troponin low-affinity sites)	k_+^{TN}	39 μM^{-1} s^{-1}	Robertson et al., 1981
Ca^{2+} off-rate constant (troponin low-affinity sites)	k_-^{TN}	20 s^{-1}	Robertson et al., 1981
Ca^{2+} dissociation constant (troponin low-affinity sites)	K_D^{TN}	0.5 μM	Robertson et al., 1981
Ca^{2+} on-rate constant for calmodulin	k_+^{CAL}	125 μM^{-1} s^{-1}	Soeller and Cannell, 1997
Ca^{2+} off-rate constant for calmodulin	k_-^{CAL}	297.5 s^{-1}	Estimated
Ca^{2+} dissociation constant for calmodulin	K_D^{CAL}	2.38 μM	Robertson et al., 1981
Ca^{2+} on-rate constant (phospholipid low-affinity sites)	k_+^{PL}	125 μM^{-1} s^{-1}	Soeller and Cannell, 1997
Ca^{2+} off-rate constant (phospholipid low-affinity sites)	k_-^{PL}	1375×10^2 s^{-1}	Estimated
Ca^{2+} dissociation constant (phospholipid low-affinity sites)	K_D^{PL}	1100 μM	Langer and Peskoff, 1996
Ca^{2+} on-rate constant (phospholipid high-affinity sites)	k_+^{PH}	125 μM^{-1} s^{-1}	Soeller and Cannell, 1997
Ca^{2+} off-rate constant (phospholipid high-affinity sites)	k_-^{PH}	1625 s^{-1}	Estimated
Ca^{2+} dissociation constant (phospholipid high-affinity sites)	K_D^{PH}	13 μM	Langer and Peskoff, 1996
Ca^{2+} on-rate constant for Fluo-3	k_+^{FLUO}	230 μM^{-1} s^{-1}	Eberhard and Erne, 1989
Ca^{2+} off-rate constant for Fluo-3	k_-^{FLUO}	170 s^{-1}	Eberhard and Erne, 1989
Ca^{2+} dissociation constant for Fluo-3	K_D^{FLUO}	0.739 μM	Eberhard and Erne, 1989
Ca^{2+} on-rate constant for ATP*	k_+^{ATP}	225 μM^{-1} s^{-1}	Baylor and Hollingworth, 1998
Ca^{2+} off-rate constant for ATP*	k_-^{ATP}	45000 s^{-1}	Baylor and Hollingworth, 1998
Ca^{2+} dissociation constant for ATP*	K_D^{ATP}	200 μM	Baylor and Hollingworth, 1998
L-type Ca^{2+} current parameters			
Faraday's constant	F	96.5 coulomb $mmol^{-1}$	
Constant	a_1	−3.857 pA/pF	Fit to experiment
Constant	a_2	3.5846 pA/pF	Fit to experiment
Constant	a_3	0.48185 s^{-1}	Fit to experiment
Constant	b_0	−1.161 pA/pF	Fit to experiment
Constant	b_1	−1.55 pA/pF	Fit to experiment
Constant	b_2	0.0081376 s^{-1}	Fit to experiment
Constant	b_3	−1.6235 pA/pF	Fit to experiment
Constant	b_4	0.0079641 s^{-1}	Fit to experiment
Na^+/Ca^{2+} exchanger parameters			
Maximal velocity at −70 mV	$V_{max,x}$	853 μM s^{-1}	Estimated
Maximal velocity at 0 mV	$V_{max,x}$	85.3 μM s^{-1}	Estimated
Ca^{2+} concentration at half $V_{max,x}$	K_m	1 μM	Backx et al., 1989
Hill's coefficient	n	1	Backx et al., 1989

*ATP was only included in some simulations.

phospholipid rate constants for Ca^{2+} binding, the typical near-diffusion-limited value of 125 μM^{-1} s^{-1} was assumed for the low- and high-affinity phospholipid on-rate constants. The corresponding off-rate constants were calculated from the known values of the equilibrium dissociation constants (K_D^{PH}, K_D^{PL}) and on-rate constants.

Ca^{2+} buffering by the endogenous mobile buffer calmodulin (24 μM) was also included in the model because calmodulin can bind significant amounts of Ca^{2+} (Robertson et al., 1981; Fabiato, 1983). Calmodulin has four Ca^{2+} binding sites that also bind Mg^{2+}, K^+, and Na^+. Fabiato (1983) reported two classes of Ca^{2+} binding sites on calmodulin (low- and high-affinity), and Robertson et al. (1981) suggested that the properties of all calmodulin metal-binding sites are similar to the Ca^{2+}-specific sites on troponin. In our paper, we assumed that all four calmodulin binding sites were similar. The calmodulin equilibrium dissociation constant (K_D^{CAL} = 2.38 μM) was taken from Robertson et al. (1981). The value of the off-rate calmodulin constant was calculated assuming that the on-rate constant has a value of 125 μM^{-1} s^{-1}.

During the experiment the atrial myocyte was loaded with 100 μM fluorescent Ca^{2+}-indicator (Fluo-3). In skeletal muscle, Fluo-3 was found to strongly bind to cellular constituents, giving rise to a total Fluo-3 concentration that is higher than in the pipette filling solution (Harkins et al., 1993). Indeed, confocal images of skeletal muscle cells loaded with Fluo-3 show a clear striation pattern, indicative of dye binding. However, in both ventricular and atrial cardiac muscle cells, a striation pattern is not observed, suggesting that Fluo-3 binding is less pronounced in these cells. Further support for this notion was obtained when cardiac myocytes were permeabilized and only 4% of the dye was found to be irreversibly bound (Lipp et al., 1996), at least when the Ca^{2+}-indicator was loaded in the salt form via a patch-clamp pipette. Thus, as an approximation we used a concentration of 100 μM Fluo-3 in our analysis. The Ca^{2+} dissociation constant for Fluo-3 was (K_D^{FLUO} = 0.739 μM) and the Ca^{2+} on- and off-rate constants were (k_+^{FLUO} = 230 μM^{-1} s^{-1}, k_-^{FLUO} = 170 s^{-1}) (Eberhard and Erne, 1989; Ellis-Davies et al., 1996). In this study we also examined how Ca^{2+} binding by the endogenous low-affinity mobile Ca^{2+} buffer ATP might influence the intracellular Ca^{2+} signals in atrial myocytes. The ATP concentration in the pipette was 5 mM. With 1 mM Mg^{2+} added, free ATP is calculated to be 260 μM. During our simulations, the amount of ATP able to bind Ca^{2+} was therefore assumed to be 260 μM (i.e., ~5% of 5 mM total ATP), because [MgATP] is known to remain almost constant despite some changes in $[Ca^{2+}]_i$. The ATP dissociation constant (K_D^{ATP} = 200 μM) and Ca^{2+} on- and off-rate constants (225 μM s^{-1} and 45,000 s^{-1}) were taken from Baylor and Hollingworth (1998) and recalculated to account for 22°C (i.e., k_+^{ATP} = 1.5 × 150 μM s^{-1} and k_-^{ATP} = 1.5 × 30,000 s^{-1}). We also assumed that ATP binds only Ca^{2+} and Mg^{2+} and that the binding of ATP to different immobile structures (proteins, organelles) within the cell is not able to noticeably change the total ATP amount (Kushmerick and Podolsky, 1969).

Ca^{2+} and buffer diffusion coefficients

The diffusion coefficient for Ca^{2+} in the restricted subsarcolemmal space has been reported to be 350 μm^2 s^{-1} in the *r*-direction (i.e., ~0.5-fold that in water because of the viscosity of the cytoplasm) and ~140 μm^2 s^{-1} in the longitudinal *z*-direction (i.e., further reduced by the presence of the "foot" structures; Soeller and Cannell, 1997). Because our model only simulates radial diffusion and assuming that there is water in the restricted space, the diffusion coefficient for Ca^{2+} used there was 780 μm^2 s^{-1}.

Gabso et al. (1997) assessed the values for the average diffusion coefficient of the endogenous buffers (calmodulin, calbindin) in the cytoplasm to be between 14 and 20 μm^2 s^{-1}. In our model the diffusion coefficient for calmodulin (as CaCAL) in the MYOF was assumed to be 25 μm^2 s^{-1}. The diffusion coefficient for Fluo-3 (as CaFLUO), which resulted in the best agreement with the experimental data, turned out to be 100 μm^2 s^{-1}. This estimated diffusion coefficient is fivefold larger than what has been measured in skeletal muscle (Harkins et al., 1993), in agreement with the assumption that Fluo-3 does not strongly bind to cellular constituents in atrial cardiac myocytes. It corresponds to the diffusion coefficient in water, with a correction for intracellular viscosity (Klingauf and Neher, 1997). The diffusion coefficient for ATP (as CaATP) in the MYOF (168 μm^2 s^{-1}) was taken from Baylor and Hollingworth (1998) and adjusted for 22°C (i.e., =1.2 × 140 μm^2 s^{-1}).

To solve the system of diffusion equations numerically, the explicit finite-difference method described by Crank (1975) was used. The boundaries between the extracellular space and the RSP and the MYOF and the RSP, where the diffusion coefficients for Ca^{2+}, Fluo-3, and calmodulin change, were treated as described for the diffusion through composite media. Taking the cylindrical symmetry of the problem into account, the system of equations was solved on a one-dimensional nonlinear grid. The radial step size for integration was 77 nm in MYOF and 6 nm in RSP. The interval for the integration was 10^{-8} s. Because of the complex nature of the calculations, they had to be carried out on a VAX mainframe computer (University Computing Center, Bern, Switzerland). Unless specified otherwise in the figure legends or in the text, the standard set of parameters was used in the simulations, as listed in Table 1.

RESULTS

Experimental recordings of Ca^{2+} influx and changes of $[Ca^{2+}]_i$

The voltage-clamp protocol elicited inward currents with the typical signatures of the L-type Ca^{2+} current (Fig. 1 *D*). At the onset of the first voltage step from −70 to −40 mV a small current was observable, most likely attributable to incomplete blockade of Na^+ channels by 10 μM TTX. In all cases a Ca^{2+} signal due to Ca^{2+} influx accompanied the inward current that coincided with the second voltage step from −40 to 0 mV, and thus corresponded to the activation of the L-type Ca^{2+} current. The Ca^{2+} current and the Ca^{2+} signal resulting from the Ca^{2+} influx were both blocked by 5 mM Cd^{2+} (data not shown). Please note that there was no Ca^{2+} release from the SR in our experiments, because the cells had been pretreated with ryanodine and thapsigargin.

Fig. 1 also shows additional data used to develop and validate the mathematical model. Panel *A* represents a false color *x*-*y* image of cytosolic Fluo-3 fluorescence under resting conditions, which was used to determine the geometrical parameters of the cell. The bright spot marks the tip of the patch-clamp pipette. This cell had a length of 125 μm, a diameter of 15.6 μm, and a membrane capacitance of 41 pF.

A typical line-scan image acquired during a voltage-clamp protocol along the entire width of the cell is shown in Fig. 1 *E*. The colors correspond to fluorescence ratio values (F/F_0) reflecting the changes of Ca^{2+} concentration in time (vertical dimension of the image). A clear U-shaped profile extending across the cell is visible at the beginning of the Ca^{2+} signal resulting from Ca^{2+} influx (see also Fig. 1 *F*). A convenient way to visualize the relationship among space, time, and Ca^{2+} concentration is provided by the surface plot (panel 1 *G*). In this representation it is readily appreciable that the Ca^{2+} concentration increased faster and to a higher amplitude at the edges of the cell for a given time point, whereas in the center of the cell the signal reached a similar amplitude only after a considerable delay.

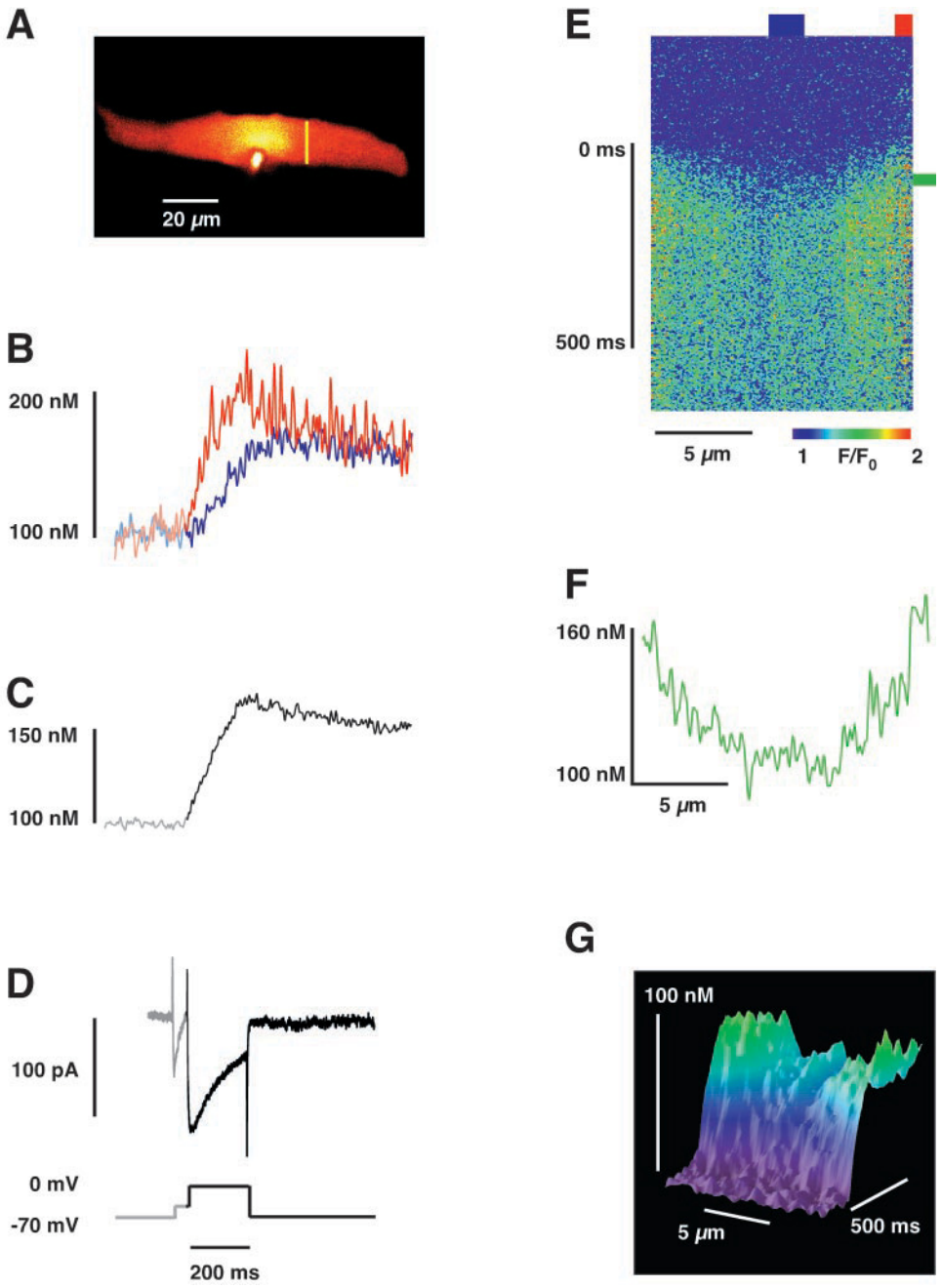

FIGURE 1 Ca^{2+} current and Ca^{2+} concentration recorded from an isolated guinea pig atrial myocyte (*A*), loaded with 100 μM Fluo-3 by dialysis from a patch-clamp pipette. A single line (*yellow line* in *A*) was then scanned to obtain a line-scan image of fluorescence versus space and time (*E*). (*B*) The time course of $[Ca^{2+}]_i$ was obtained for the periphery (*red*) and center (*blue*) of the cell. Panel (*C*) shows the Ca^{2+} transient averaged along the complete line-scan image. The voltage-clamp protocol and the resulting L-type Ca^{2+} current are illustrated in (*D*). The spatial profile of $[Ca^{2+}]_i$ is shown in (*F*), while (*G*) shows a surface plot computed from the line-scan image in (*E*). The red, green and blue bars in (*E*) indicate the region from which traces were averaged. Note that the gray portions of the traces in panels *B–D* belong to the pre-pulse protocol and where not simulated in the model.

In Fig. 1 *B* the Ca^{2+} concentration changes extracted from the periphery (*red*) and the center of the line-scan image (*blue*) are superimposed to emphasize the delay between the two signals. The time course of the average Ca^{2+} concentration (calculated by averaging all points along the line-scan) is plotted in Fig. 1 *C*. The duration of the rising phase (200 ms) of the Ca^{2+} signal from the edge of the cell (*red trace* in Fig. 1 *B*) matched the duration of the L-type Ca^{2+} current. In contrast, the Ca^{2+} signal recorded from the center (*blue*) developed more slowly and continued to rise even when the current was already terminated.

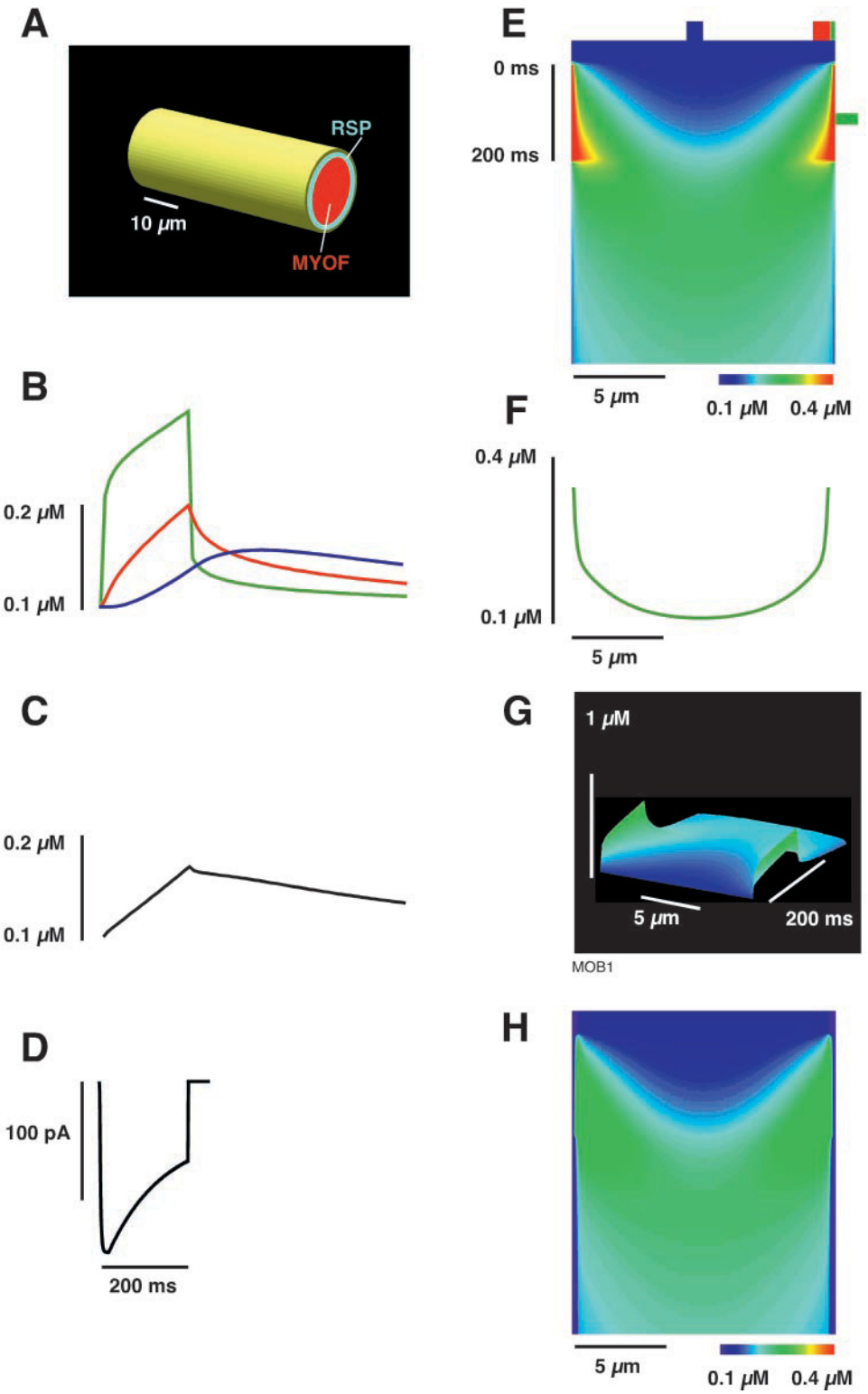

FIGURE 2 Simulating the experimental data with the computer model. Panel (*A*) depicts the cylindrical model cell containing a myofilament space (MYOF) surrounded by a space with restricted diffusion (RSP). The radius of the cell was 7.8 μm, the thickness of RSP was 20 nm (unless noted otherwise). The length of the cylinder was adjusted to accommodate the accessible volume of the cytosol (~50% of total cytosolic volume in this case). The time courses of the Ca^{2+} concentration in the center (*blue line*) and in the RSP (*green line*) are superimposed in (*B*). In addition, the Ca^{2+} profile averaged over the first micrometer under the membrane is shown in red. This approximately corresponds to confocal recordings of Ca^{2+} in the cell periphery. Panel (*C*) shows the time course of the Ca^{2+} concentration averaged over the entire cell. The simulated Ca^{2+} influx, corresponding to the L-type Ca^{2+} current in Fig. 1, is illustrated in (*D*). The Ca^{2+} concentration changes were also visualized as line-scans (*E*) and as surface plots (*G*). From the line-scan image the time course traces and the Ca^{2+} concentration profile at 100 ms (*F*) were extracted and colored according to the respective symbols. Panel (*H*) was computed by convolving a simplified confocal point-spread function with the image shown in (*E*). This mimicks the limited optical resolution present in experimental data (compare with Fig. 1 *E*).

Numerical simulation of the experimental data

The first set of modeling results (Fig. 2) describes our attempt to create a simulation that quantitatively approximates the experimental data. Fig. 2, *A–G* are arranged in analogy to the experimental Fig. 1; Fig. 2 *H* was obtained by convolving the model data with a simplified confocal point-spread function. Thus Fig. 2, *E*, *G*, and *H* illustrate the calculated temporal and spatial Ca^{2+} concentration changes as line-scan images and as a surface plot. The simulated

local Ca^{2+} signals in the center (*blue*) and periphery (*red*) are shown in Fig. 2 *B*. The Ca^{2+} signal in the cell periphery was calculated by averaging the Ca^{2+} concentration across the first micrometer under the membrane. This average corresponds to the experimental measurement of peripheral $[Ca^{2+}]$, which is also a spatial average due to the limited optical resolution. As expected, the convolution of the simulated data with the point-spread function eliminated the signal in the fuzzy space and also introduced some edge effects at the boundary of the line-scan. These model results illustrate that the Ca^{2+} signal in the cell periphery increases faster and has a larger amplitude than the Ca^{2+} signal in the center, which peaks with a delay of ~100 ms. The simulations also suggest that the slower and smaller Ca^{2+} transient in the center can be explained by diffusion of Ca^{2+}. The Ca^{2+} influx carried by the simulated Ca^{2+} current allowed us to predict the Ca^{2+} concentration levels developed in the narrow fuzzy space (RSP) that is not accessible experimentally (Fig. 2 *B*, *green line*). Thus, the model predicts steep Ca^{2+} concentration gradients within the signals recorded experimentally from the cell periphery. The simulated U-profile of Ca^{2+} at 100 ms extracted from the line-scan image (Fig. 2 *E*) is shown in Fig. 2 *F*. Note that, in contrast to the experimentally measured signal (Fig. 1 *F*), the calculated Ca^{2+} concentration near the plasmalemma peaks at 244 nM above resting concentration because the model is able to predict Ca^{2+} concentrations in the narrow RSP, which cannot be resolved optically. Fig. 2 *C* shows a Ca^{2+} transient averaged across the entire cell corresponding to the experimentally measured signal (Fig. 1 *C*).

The good agreement between the theoretical and the experimental data suggested that the model, as implemented, correctly described the subcellular Ca^{2+} signaling in atrial myocytes. Furthermore, these quantitatively correct results provided an opportunity to examine and better understand how different model parameters beyond the experimentally accessible limits might influence the spatial and temporal characteristics of the Ca^{2+} transients.

Exploring the parameter space

Accessible volume fraction

The subcellular aqueous volume accessible to Ca^{2+} represents an important but not precisely known scaling factor for the amplitude of the Ca^{2+} signals. In the next set of simulations we sought to determine the role of the accessible volume fraction. The spatial and temporal Ca^{2+} concentration changes calculated in response to the L-type Ca^{2+} current (Fig. 2 *D*) for an accessible volume fraction of ~70% are shown in Fig. 3 *A* (compare with Fig. 2 *G* where $V_{acc} \sim 50\%$). A subcellular aqueous volume of 70% assumes that 1) the nuclei are accessible for Ca^{2+}; 2) the mitochondria are not accessible for Ca^{2+}; 3) the SR is accessible for Ca^{2+}, i.e., SR Ca^{2+} release channels are open and Ca^{2+} would even be able to go backward into the SR during the cytosolic Ca^{2+} transient; and 4) the myofilament space contains 75% water. The local Ca^{2+} transients obtained for V_{acc} ~70% (*solid lines*) and those for a volume of 50% (*dashed lines*) are superimposed in Fig. 3 *B*. The Ca^{2+} U-profiles at 100 ms can be compared in Fig. 3 *C*. These model results reveal that the increased accessible volume fraction reduces cytosolic Ca^{2+} concentrations in all simulated cytosolic layers, as expected. Variable scaling of the cell length allowed us to keep the cylindrical cell shape, the diameter, and the total buffer capacity of the model cell constant, while simulating different accessible volumes. For numerical simulations of different concentrations for calmodulin, troponin C, and Fluo-3, see below.

Buffer mobility

A number of theoretical and experimental studies (Zhou and Neher, 1993; Wagner and Keizer, 1994; Jafri and Keizer, 1995; Gabso et al., 1997; Baylor and Hollingworth, 1998; Jiang et al., 1999; Tang et al., 2000) suggest that mobile buffers tend to increase the diffusion of Ca^{2+} while the stationary buffers retard Ca^{2+} transport in the cell. The conjecture made in the present model, that the endogenous calmodulin and the exogenous Fluo-3 are mobile Ca^{2+} buffers, allowed us to examine how the mobility of these buffers would affect the Ca^{2+} dynamics in atrial myocytes. Fig. 3 *D* shows a simulation in which all Ca^{2+} buffers were made stationary. It is striking that under these conditions Ca^{2+} only diffused slowly to the center of the cell and essentially remained near the cell membrane during the analyzed interval, resulting in a high local Ca^{2+} concentration in the RSP (compare with Fig. 2 *G*, where Fluo-3 and calmodulin were mobile with $D_{MYOF}^{CaFLUO} = 100\ \mu m^2\ s^{-1}$ and $D_{MYOF}^{CaCAL} = 25\ \mu m^2\ s^{-1}$).

Fluo-3 concentration

The inclusion of the Ca^{2+} indicator Fluo-3 in the model provided a possibility to examine and analyze how different Fluo-3 concentrations would affect the Ca^{2+} signals in atrial myocytes. For this purpose Ca^{2+} signals arising from influx via L-type Ca^{2+} current were simulated for Fluo-3 concentrations ranging from 0 μM to 1600 μM. The surface plots in Fig. 4, *A–C* reveal that the Ca^{2+} indicator has a pronounced effect on the Ca^{2+} mobility. In addition, our model results (Fig. 4 *D*) illustrate that 1) at low concentrations, Fluo-3 accelerates the spread of the Ca^{2+} signal toward the center because the CaFLUO complex carries a sizeable amount of Ca^{2+}; 2) at concentrations above ~50 μM, Fluo-3 suppresses the Ca^{2+} signal in the center because the buffering capacity of the Ca^{2+} indicator dye becomes dominant. The calculated Ca^{2+} concentrations at 100 ms versus different Fluo-3 concentrations in the RSP (*red*), periphery

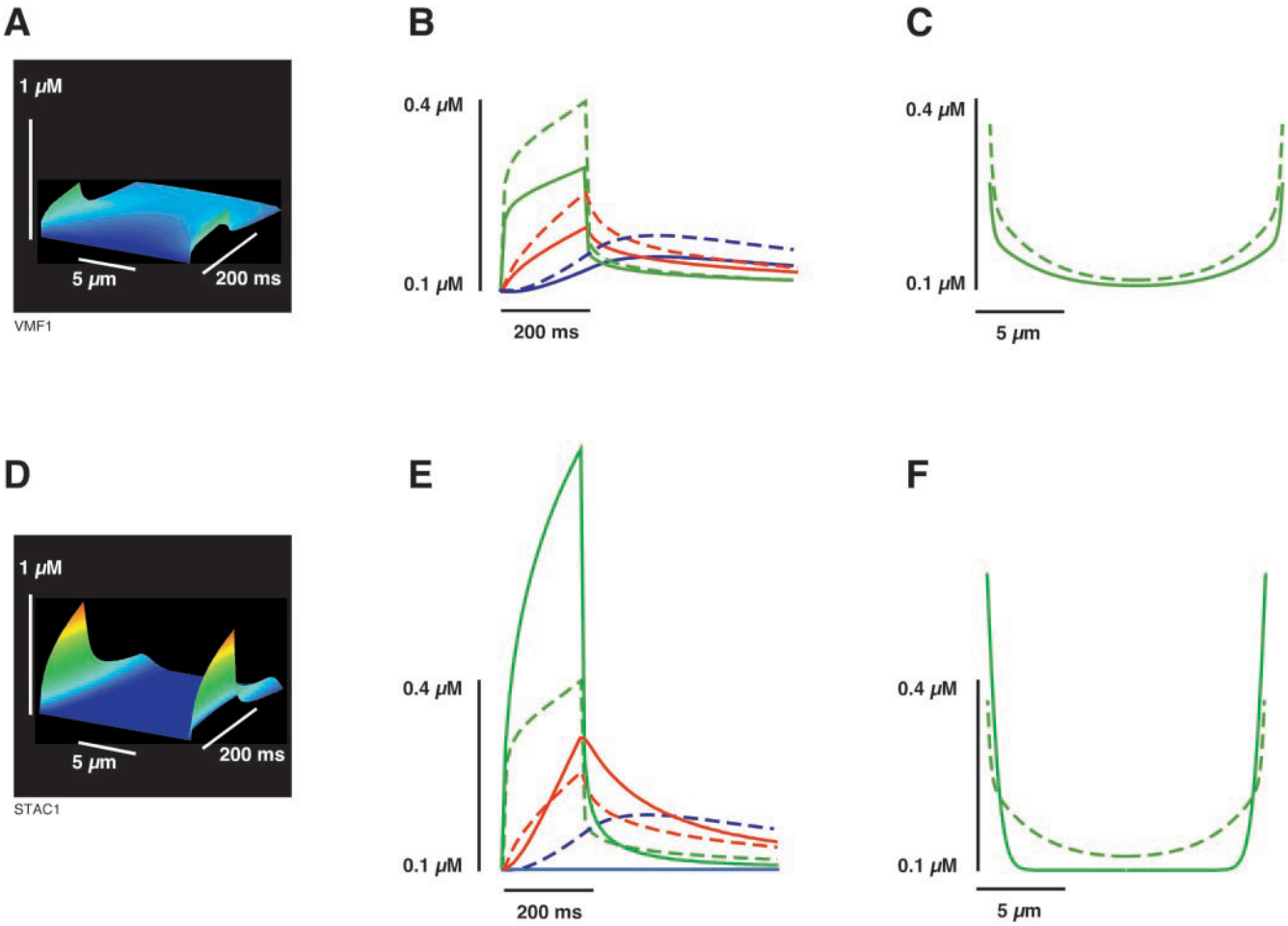

FIGURE 3 Effects of changes in the accessible volume fraction and buffer mobility. Different estimates of the accessible volume fraction are compared in (*A–C*). (*A*) The surface plot obtained for an accessible volume of 70% of the total cell volume (compare also with Fig. 2 *G*, where accessible volume was 50%). In (*B*) Ca^{2+} profiles are shown for the cell center (*blue*), restricted space (*green*), and periphery (*red*). (*C*) The Ca^{2+} profile at 100 ms. These signals are compared with those from a volume of 50% (*dashed lines* in (*B*) and (*C*)). In panels (*D–F*) we illustrate the effect of buffer mobility. Panel (*D*) represents a surface plot when all buffers remain stationary (compare with Fig. 2 *G*, where Fluo-3 and calmodulin were mobile). (*E*) and (*F*) allow a quantitative comparison of the effects of buffer mobility. The color-coding is identical to (*B*) and (*C*). The Ca^{2+} signal in the center is dramatically slowed down while the Ca^{2+} concentration in the restricted space reaches much larger values when the buffers are immobilized.

(*green*), and the cell center (*blue*), and for the averaged concentration (*black*) are shown in Fig. 4 *E*.

ATP as a mobile Ca^{2+} buffer

Another important advantage of our simulation was the ability to predict the Ca^{2+} signals that would occur in the absence of Fluo-3. Model simulations performed under such conditions revealed that at zero Fluo-3 and only calmodulin as a mobile buffer Ca^{2+} diffusion to the cell center would be extremely slow (Fig. 4, *A* and *D*). In the absence of Fluo-3 a Ca^{2+} peak is not reached in the center even after 700 ms, despite the presence of the mobile buffer calmodulin. What could be possible explanations for this result? It has been reported recently that in smooth muscle cells (Kargacin and Kargacin, 1997) and in skeletal muscle cells (Baylor and Hollingworth, 1998) the low-affinity mobile Ca^{2+} buffer ATP could significantly affect the amplitude and time course of intracellular Ca^{2+} signals. To test this possibility we included a simplified equation for the kinetics and diffusion of ATP in our model (as CaATP).

The Ca^{2+} signals calculated in response to an L-type Ca^{2+} current, when 260 μM mobile ATP were included together with 24 μM mobile calmodulin and zero Fluo-3, are shown in Fig. 4, *F* and *G*. The simulation results predict a significant acceleration of Ca^{2+} diffusion (compare with Fig. 4, *A*, where only calmodulin is mobile and Fluo-3 = 0 μM). A free ATP concentration of 260 μM assumes 5 mM total ATP with 95% MgATP and 5% free ATP. The quantitative comparison of the effect of ATP (restricted space, periphery, center) and an expanded view of the cell center are shown in Fig. 4, *F* and *G*. These simulations clearly

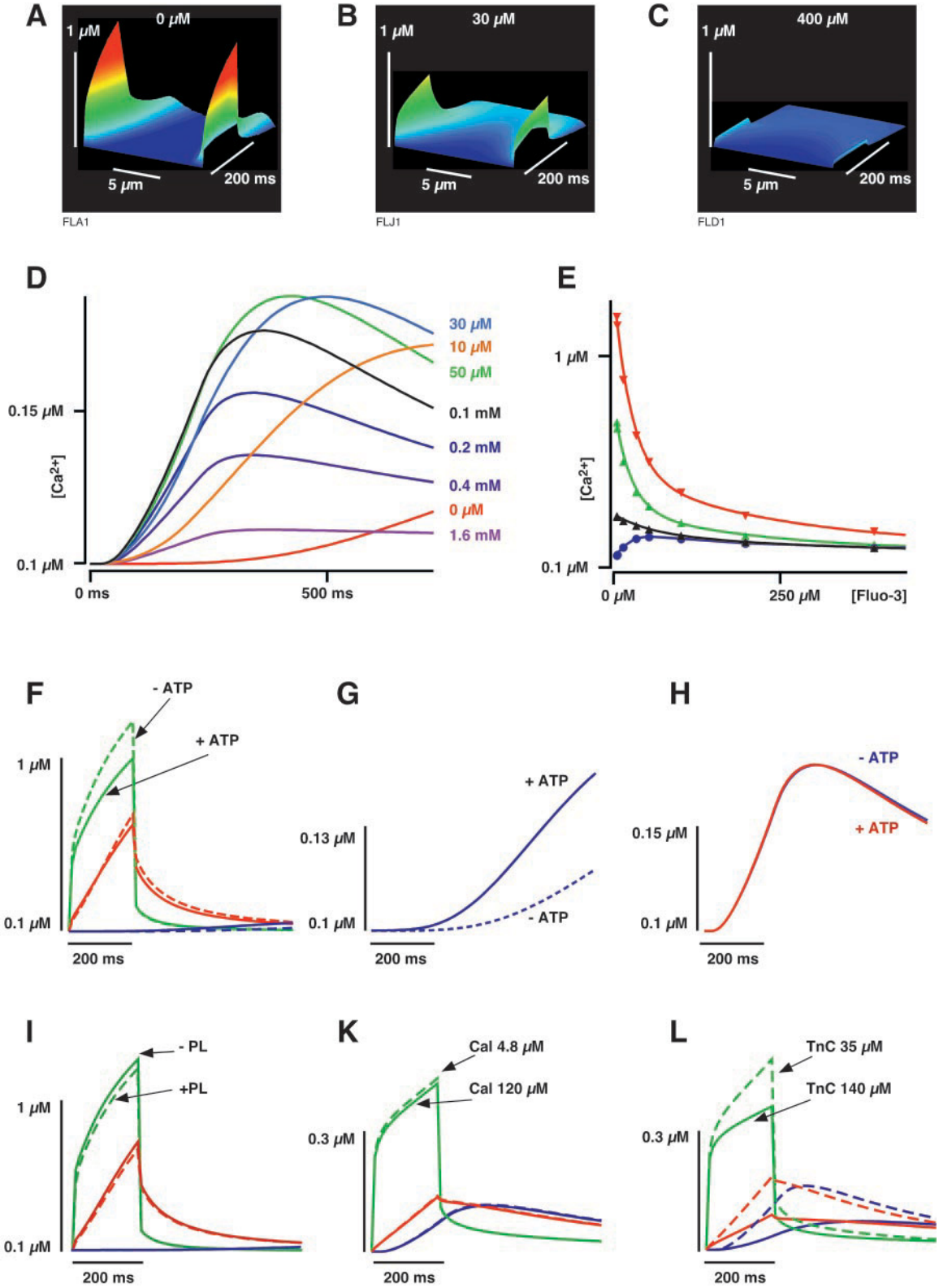

FIGURE 4 Effect of Fluo-3 concentration, ATP concentration, and presence of phospholipids on the sarcolemma. Surface plots were constructed from simulations with different concentrations of the mobile Ca^{2+} buffer Fluo-3 (*A*, 0 μM; *B*, 30 μM; *C*, 400 μM). The time course of the Ca^{2+} concentration in the center of the cell is illustrated in (*D*) for Fluo-3 concentrations from 0 μM to 1600 μM. Two effects of Fluo-3 become apparent: 1) at low concentrations, Fluo-3 accelerated the Ca^{2+} signal in the cell center because it carries bound Ca^{2+} while it diffuses; 2) at high concentration, the Ca^{2+} signals are suppressed because the buffering capacity of Fluo-3 dominates. This is also evident in (*E*) where the Ca^{2+} concentration at 100 ms is shown

reveal that 260 μM ATP was able to dramatically influence the amplitude and the time course of the Ca^{2+} signals. This was not the case when ATP was simulated to be immobile (data not shown). However, in the presence of 100 μM Fluo-3 and 24 μM calmodulin, adding ATP only slightly accelerated the Ca^{2+} in the center (Fig. 4 *H*).

The model also predicts that in the presence of Fluo-3 Ca^{2+} binding and diffusion of the poorly mobile Ca^{2+} buffer calmodulin would not significantly influence the amplitude and time course of the global intracellular Ca^{2+} signals. Our studies revealed that under these conditions fivefold increases or decreases of the calmodulin concentration only had a limited effect on the calculated Ca^{2+} signals (Fig. 4 *K*).

However, when we imposed twofold changes in the concentration of the stationary buffer troponin C, much more pronounced alterations of the Ca^{2+} signals resulted (see Fig. 4 *L*). While the Ca^{2+} signal in the restricted space was attenuated noticeably, the effect was even more pronounced in the center of the cell, and was paralelled by a delayed time course of the Ca^{2+} signal.

The fuzzy space

An additional goal of the present study was to use the model to examine the importance of mobile and stationary Ca^{2+} buffers, and the impact of the restricted space geometry, on the Ca^{2+} signals arising within the narrow fuzzy space (~20 nm) that is below the optical resolution of confocal microscopes.

Mobile Ca^{2+} buffers in the restricted space

Several simulations indicated that the mobile Ca^{2+} buffers Fluo-3 and ATP may significantly affect the Ca^{2+} signals in the fuzzy space: 1) the immobilization of Fluo-3 (or ATP) significantly increased Ca^{2+} signals in the fuzzy space (Fig. 3, *D–F*, Fig. 4, *A*, *F*, and *G*); 2) raising the Fluo-3 concentration from 0 μM to 1600 μM blunted Ca^{2+} transients in the fuzzy space (Fig. 4 *E*). Additional simulations revealed that in the presence of 100 μM Fluo-3 the Ca^{2+} buffer calmodulin was not able to significantly affect the Ca^{2+} signals in the fuzzy space, while changes in the concentration of the stationary buffer TnC had a strong effect both in the cell center and in the fuzzy space (Fig. 4, *K* and *L*).

The values for the diffusion coefficients of Ca^{2+} and mobile buffers are other important factors that might affect the calculated Ca^{2+} signals in the RSP. For the present study we assumed that there is water inside the RSP, i.e., the diffusion coefficients in the *r*-direction for Ca^{2+} and mobile buffers used (Figs. 2–4) were those in water ($D_{RSP}^{Ca} = 780$ $\mu m^2\ s^{-1}$, $D_{RSP}^{CaCAL} = 50$ $\mu m^2\ s^{-1}$, $D_{RSP}^{CaFLUO} = 200$ $\mu m^2\ s^{-1}$, $D_{RSP}^{CaATP} = 320$ $\mu m^2\ s^{-1}$). Soeller and Cannell (1997) assumed that in ventricular myocytes the diffusion coefficient for Ca^{2+} in the *r*-direction is ~0.5-fold that in water because of the viscosity of the cytoplasm. To test for a possible effect of D_{RSP}^{Ca} in atrial cells, the diffusion coefficient was decreased twofold (i.e., $D_{RSP}^{Ca} = 390$ $\mu m^2\ s^{-1}$) and the diffusion coefficients for the mobile buffers were also reduced twofold. During these simulations we found that variations of the diffusion coefficient on this order of magnitude had a negligible effect on the calculated Ca^{2+} signals in the RSP and on subsequent MYOF signals (data not shown).

Stationary Ca^{2+} buffers in the restricted space

During simulations of SR Ca^{2+} release into the diadic cleft, a major effect of the stationary phospholipid Ca^{2+} binding sites has been suggested (Langer and Peskoff, 1996; Soeller and Cannell, 1997; Peskoff and Langer, 1998). To examine the impact of these phospholipids on the much smaller Ca^{2+} signals in atrial myocytes (arising from Ca^{2+} influx via Ca^{2+} current only), we included them in our model. The Ca^{2+} signals shown in Fig. 4 *I* indicate that during Ca^{2+} influx alone the phospholipids had only a limited effect on the calculated Ca^{2+} signals (0 μM Fluo-3, 260 μM ATP, 24 μM calmodulin). The effect was even smaller when 100 μM Fluo-3 was included (data not shown).

Restricted space geometry

Gomez et al. (1997) hypothesized that an altered geometry of the diadic space could affect E-C coupling during congestive heart failure. To examine how changes of the restricted space volume would modify the Ca^{2+} transient, we computed these signals while reducing the restricted space thickness (d_{RSP}) from 20 nm to 12 nm. Our simulations revealed that these changes of the restricted space volume had no noticeable effect on the calculated Ca^{2+} signals in

at various Fluo-3 concentrations for the restricted space (*red*), the periphery (*green*), the average (*black*), and the cell center (*blue*). In the center, the dual effect of Fluo-3 leads to low Ca^{2+} at both low and high Fluo-3 concentrations. Panels (*F–G*) show the effect of the mobile Ca^{2+} buffer ATP in the absence of Fluo-3. Panel (*F*) allows a quantitative comparison of the effect of ATP. Panel (*G*) is an expanded view of the cell center from (*F*). ATP significantly accelerates Ca^{2+} diffusion in the absence of Fluo-3. In the presence of 100 μM Fluo-3, the effect of ATP is minimal (*H*). The buffering by the stationary low-affinity phospholipids becomes evident in the restricted space, at least in the absence of Fluo-3, panel (*I*). A fivefold increase or reduction of the calmodulin concentration only exhibited a minimal effect (*K*), while even smaller alterations of the TnC concentration were accompanied by pronounced effects (*L*).

the RSP (data not shown). Furthermore, when the RSP was omitted completely, the Ca^{2+} transients in the center of the cell did not change noticeably.

DISCUSSION

As defined in the Introduction, the aims of this study were threefold: 1) to develop a computer model of Ca^{2+} signaling and diffusion and to validate this model by simulating our own experimental results quantitatively; 2) to use this model to predict and analyze Ca^{2+} signals in subcellular spaces that are too small to be resolved experimentally (i.e., in the subsarcolemmal fuzzy space); and 3) to examine the role of the mobile buffer and even simulate experiments that cannot be performed because of technical reasons (for example, examining Ca^{2+} transients in the absence of a Ca^{2+} indicator).

Experimental data

For our first goal, to simulate Ca^{2+} signals that would quantitatively correspond to our experimental data, we were trying to use a cardiac myocyte preparation that would have little spatial complexity. For this purpose, atrial cardiac myocytes appeared to be ideal because they are known to exhibit a less complex ultrastructure than ventricular cells, mostly because they do not contain T-tubules (Bers, 2001). This feature results in a simplified spatial pattern of Ca^{2+} influx and diffusion in a cell that can reasonably well be approximated by assuming a cylindrical shape. Because our aim was to develop a model that would allow us to study Ca^{2+} entry and diffusion, we performed all experiments on atrial cells that had been pretreated with ryanodine and thapsigargin to eliminate the SR as a system for Ca^{2+} uptake and release via Ca^{2+}-induced Ca^{2+} release. The recorded Ca^{2+} signals were consistent with Ca^{2+} first entering through L-type Ca^{2+} channels in the plasmalemma, followed by diffusion of Ca^{2+} toward the center of the cell, giving raise to a U-shaped profile of Ca^{2+} concentration. This U-shaped profile was only observed when the temporal resolution was sufficiently high (2 ms/line). The absence of Ca^{2+} signal amplification by CICR was also confirmed by the small Ca^{2+} signal peaking at 60 nM above resting concentration.

Because L-type Ca^{2+} current and cytosolic Ca^{2+} concentration were recorded simultaneously, we obtained quantitative information on Ca^{2+} influx (i.e., by integrating the amount of charge entering during the Ca^{2+} current) and on the resulting change of the cytosolic Ca^{2+} concentration. From the confocal optical section and from three-dimensional confocal optical data we could approximate the total cell volume (i.e., the volume occupied by Fluo-3). When assuming a fraction of the cell volume that was actually accessible to the Ca^{2+} entering the cell during the Ca^{2+} current, we could estimate the buffering capacity of the cytosol for Ca^{2+} (defined as change of free $[Ca^{2+}]_i$ for a given total Ca^{2+} concentration; see below for a discussion on estimates of accessible cell volume). As it turned out, the buffer capacity was 7.6 nM/1 μM (or 1:131) when assuming an accessible volume fraction of ~50%, a value that falls in the range of estimates obtained with other techniques (Berlin et al., 1994). Indeed, using buffer concentrations taken from the literature, the best quantitative agreement with our experimental data was obtained when performing simulations with an accessible volume of ~50%. This volume fraction implies that Ca^{2+} has no fast access to the mitochondrial space (17.9% of the cell volume) and to the interior of the SR (9.93% of the cell volume) and that 50% of the myofilament space is occupied by proteins.

The computer model

The computer model presented here was able to quantitatively simulate and reproduce our experimental results on Ca^{2+} influx, Ca^{2+} buffering, and Ca^{2+} diffusion in atrial cardiac myocytes when the SR was inhibited. The analysis of our results showed that mobile Ca^{2+} buffers (calmodulin, Fluo-3, ATP) greatly accelerate Ca^{2+} diffusion, while stationary Ca^{2+} buffers (troponin C, phospholipids) slow down the Ca^{2+} signal. This finding confirms previous studies (e.g., Zhou and Neher, 1993; Tang et al., 2000) and implies that a larger quantity of Ca^{2+} moves via diffusion of Ca^{2+}-buffer complex than as free Ca^{2+}.

In addition, the model predicts steep Ca^{2+} concentration gradients among the subsarcolemmal space, the cell periphery, and the center of the cell. Mobile Ca^{2+} buffers were able to reduce these spatial Ca^{2+} gradients. Our analysis also suggests that the subcellular aqueous volume, accessible to Ca^{2+}, represents an important but not precisely known scaling factor for the amplitude of the computed Ca^{2+} signals. Within certain limits, changing the accessible volume is equivalent to changing the concentration of Ca^{2+} buffers. This is limited to the range of Ca^{2+} concentrations in which changes of free buffer concentration remain small. Therefore, we decided to adjust the accessible volume to obtain a quantitatively correct simulation. Thus, the concentrations of Ca^{2+} binding proteins were taken from the literature and not varied in our initial simulations, despite the possibility that the published concentrations may not be perfectly precise. However, when we later varied to concentrations of calmodulin and troponin C, we only observed small changes of the Ca^{2+} signals for fivefold changes of calmodulin, while the effect of the stationary buffer troponin C was more pronounced. Thus, the troponin C concentration is a very important parameter when developing models of cardiac Ca^{2+} signaling and diffusion, while among the mobile buffers the added Ca^{2+} indicator Fluo-3 and ATP appear to be more important than the endogeneous Ca^{2+} buffer calmodulin (see below for discussion of Fluo-3 and ATP as Ca^{2+} buffers).

Because the myofibrillar and fuzzy spaces are probably morphologically different (Soeller and Cannell, 1997; Peskoff and Langer, 1998), our model cell contains two sepa-

rated spaces where free (unbuffered) Ca^{2+} ions and mobile buffers can diffuse with different diffusion coefficients. The values of 390 $\mu m^2\ s^{-1}$ and of 780 $\mu m^2\ s^{-1}$ for diffusion coefficients of free Ca^{2+} (D^{Ca}_{MYOF}, D^{Ca}_{RSP}) and published buffer diffusion coefficients and parameters were used to compare the theoretical curves with the experimental data. However, the effective diffusion of free Ca^{2+} ions in the cell will be slowed down because the exogenous and endogenous Ca^{2+} buffers and free Ca^{2+} concentrations are able to affect Ca^{2+} diffusion strikingly (Zhou and Neher, 1993; Wagner and Keizer, 1994; Jafri and Keizer, 1995; Gabso et al., 1997; Baylor and Hollingworth, 1998; Jiang et al., 1999; Tang et al., 2000). Consequently, the calculated effective (or apparent) diffusion coefficients for free Ca^{2+} in the myofibrillar and fuzzy spaces (D^{MYOF}_{app}, D^{RSP}_{app}) will be much less than 390 $\mu m^2\ s^{-1}$ or 780 $\mu m^2\ s^{-1}$, respectively. Using simplified equations, which do not account for the Ca^{2+} binding rate constants (Eqs. 15 and 16) it is possible to approximately estimate D^{MYOF}_{app} and D^{RSP}_{app}, as the maximal Ca^{2+} elevations during our experiment were sufficiently small and because we assumed in the model that diffusion coefficients for Ca^{2+}-bound and free mobile buffer forms are equal. Thus, D^{RSP}_{app} in the fuzzy space is given by (Gabso et al., 1997; Wagner and Keizer, 1994):

$$D^{RSP}_{app} = \frac{D^{Ca}_{RSP} + D^{CaCAL}_{RSP}\frac{[CAL]}{K^{CAL}_D} + D^{CaFLUO}_{RSP}\frac{[FLUO]}{K^{FLUO}_D} + D^{CaATP}_{RSP}\frac{[ATP]}{K^{ATP}_D}}{1 + \frac{[CAL]}{K^{CAL}_D} + \frac{[FLUO]}{K^{FLUO}_D} + \frac{[PL]}{K^{PL}_D} + \frac{[PH]}{K^{PH}_D} + \frac{[ATP]}{K^{ATP}_D}} \quad (15)$$

as

$$[Ca^{2+}]_i < K^{CAL}_D, K^{FLUO}_D, K^{ATP}_D$$

and D^{MYOF}_{app} in the myofibrillar space is

$$D^{MYOF}_{app} = \frac{D^{Ca}_{MYOF} + D^{CaCAL}_{MYOF}\frac{[CAL]}{K^{CAL}_D} + D^{CaFLUO}_{MYOF}\frac{[FLUO]}{K^{FLUO}_D} + D^{CaATP}_{MYOF}\frac{[ATP]}{K^{ATP}_D}}{1 + \frac{[CAL]}{K^{CAL}_D} + \frac{[FLUO]}{K^{FLUO}_D} + \frac{[TN]}{K^{TN}_D} + \frac{[ATP]}{K^{ATP}_D}} \quad (16)$$

as

$$[Ca^{2+}]_i < K^{CAL}_D, K^{FLUO}_D, K^{ATP}_D$$

Allbritton et al. (1992) report a value of 5–21 $\mu m^2\ s^{-1}$ for D_{app} for Ca^{2+} at low free $[Ca^{2+}]_i$ in the cytosolic extract when 223 $\mu m^2\ s^{-1}$ was assumed for the diffusion constant of free (unbuffered) Ca^{2+}. During these in vitro experiments Ca^{2+} sequestration by the subcellular stores and mitochondria had been inhibited, and only mobile calmodulin and stationary troponin C were present in the cytosol. Our calculations predict a value of 4.25 $\mu m^2\ s^{-1}$ for D^{MYOF}_{app} when D^{Ca}_{MYOF} was 390 $\mu m^2\ s^{-1}$ (see Eq. 16, 0 μM Fluo-3, 0 μM ATP). The simulations also indicate that D^{MYOF}_{app} would decrease to 3.14 $\mu m^2\ s^{-1}$ when D^{Ca}_{MYOF} was adjusted to 223 $\mu m^2\ s^{-1}$. Therefore, the value for D^{MYOF}_{app} (4.25 $\mu m^2\ s^{-1}$) predicted by our model is in reasonable agreement with the experimental observation in a completely different preparation.

For the fuzzy space Eq. 15 predicts a value of 0.89 $\mu m^2\ s^{-1}$ for D^{RSP}_{app} when D^{Ca}_{RSP} was 780 $\mu m^2\ s^{-1}$ or 0.52 $\mu m^2\ s^{-1}$ when D^{Ca}_{RSP} was 350 $\mu m^2\ s^{-1}$, respectively (0 μM Fluo-3, 0 μM ATP). The lower apparent diffusion coefficient in the fuzzy space was due to the presence of the phospholipids. Changes of D^{Ca}_{RSP} have a negligible effect on D^{RSP}_{app} because only a small fraction of Ca^{2+} diffuses in its free (i.e., unbound) form. Our simulations also indicate that adding 100 μM Fluo-3 accelerated the apparent Ca^{2+} diffusion in the fuzzy and myofibrillar space. In the presence of Fluo-3 D^{MYOF}_{app} was ~12 times larger and D^{RSP}_{app} ~13 times larger than without Fluo-3.

The pronounced effect of Fluo-3 on Ca^{2+} mobility

The simulations allowed us to vary the concentrations of all mobile and stationary Ca^{2+} buffers without restrictions and to exploit a large parameter space. We used this possibility to explore several scenarios. Initially, it was analyzed how various Fluo-3 concentrations affect the Ca^{2+} signals. These simulations revealed several distinct effects of Fluo-3. As expected and known from previously published

reports (Zhou and Neher, 1993; Wagner and Keizer, 1994; Jafri and Keizer, 1995; Gabso et al., 1997), increasing the concentration of the Ca^{2+} indicator reduced the amplitude of the resulting Ca^{2+} signal dramatically due to Ca^{2+} buffering. This effect was more pronounced in the subsarcolemmal space than in the remainder of the cytosol, presumably because the RSP does not contain the immobile Ca^{2+} buffer troponin. There is, however, experimental evidence that within the diadic cleft of ventricular myocytes, even strong buffering with high concentrations of Fura-2 and EGTA cannot interrupt E-C coupling (Adachi-Akahane et al., 1996), supporting the idea that local control of E-C coupling occurs on microdomains that are even smaller than the spatial resolution of the present mathematical model. Alternatively, the diffusion barrier of the diadic cleft may be much more pronounced locally than the change in diffusion between fuzzy space and cytosol used in the present model calculations. Such a strong diffusion barrier would most likely prevent even high cytosolic buffer concentrations from significantly interfering with signal transduction. Regarding the overall mobility of Ca^{2+}, our simulations with very low or even without Fluo-3 yielded unexpected results. When the Fluo-3 concentration was reduced or even lowered to zero, the Ca^{2+} concentration reached in the fuzzy space rose dramatically. In contrast, the time course of the Ca^{2+} signal in the center of the cell was slowed down extremely. In fact, slowing was so dramatic that such a signaling pathway could not possibly fulfil its physiological role (i.e., generate Ca^{2+} transients with a frequency corresponding to the heart rate).

How could we solve or explain this apparent dilemma? The first possibility would be the notion that this slow propagation of the Ca^{2+} signal is the reason why atrial cells have developed SR, not only near the sarcolemma, but also throughout the cell. The Ca^{2+} signal could then spread from the periphery to the cell center as a concentric reaction-diffusion wave driven and accelerated by CICR. Indeed, this is exactly what can be observed experimentally (Hüser et al., 1996; MacKenzie et al., 2001; Kockskämper et al., 2001). Another obvious possibility was that our model may be incomplete and lack, for example, some mobile Ca^{2+} buffers. It has recently been proposed that ATP may act as a significant Ca^{2+} buffer in skeletal muscle cells (Baylor and Hollingworth, 1998). Despite its low affinity for Ca^{2+} ($K_d = 200\ \mu M$), the high concentration of ATP may provide significant amounts of mobile Ca^{2+} buffer. Indeed, our simulations revealed that in the absence of Fluo-3, ATP drastically enhanced the mobility of Ca^{2+}. Adding ATP reduced the Ca^{2+} concentration reached in the subsarcolemmal space (by Ca^{2+} buffering), but accelerated Ca^{2+} movement to the cell center. The model studies also suggest that, in the presence of 100 μM Fluo-3 in the cell, Ca^{2+} binding by ATP is not very important quantitatively, at least during the Ca^{2+} concentrations reached in the present experimental study without SR Ca^{2+} release. Therefore, our previous simulations without ATP (but with 100 μM Fluo-3) remain perfectly valid, but when there is no Ca^{2+} indicator dye in the cell (i.e., under physiological conditions), mobile ATP may be important for Ca^{2+} signaling. In addition, most likely the cells contain other small and highly mobile Ca^{2+} binding molecules that are not included in the model (and may not yet have been identified).

The fuzzy space

The existence of a fuzzy space has been proposed to explain the necessary Na^+ concentration changes required to activate the Na^+-Ca^{2+} exchange after influx of Na^+ via I_{Na} (Leblanc and Hume, 1990). Although the diadic cleft seemed to be an appropriate morphological equivalent, this has never been directly demonstrated and diffusion has been suggested to be sufficiently slow to give rise to the predicted high concentrations near the sarcolemma. With the present model we were able to confirm this notion. In addition, our theoretical studies showed that the changes in the diffusion coefficients and fuzzy space geometry have little effect on the cellular Ca^{2+} transient, as recorded from the entire cell. Therefore, we concluded that the inclusion of the fuzzy space in the model was not required to simulate our experimental data. From this result we can derive that the functional importance of the RSP mainly lies in the immediate vicinity of the sarcolemma, where all membrane proteins and sarcolemmal ion channels are located. Thus, the model can be used to predict functionally relevant Ca^{2+} signals that are "seen" by these proteins.

It has been suggested for a long time that the phospholipids located in the inner layer of the sarcolemmal bilayer could represent a functionally important stationary Ca^{2+} buffer (for example see Burt and Langer, 1983; Langer and Rich, 1986). However, it has commonly been assumed that these buffers exhibited a low Ca^{2+} affinity in the millimolar range, a concentration that is unlikely to prevail inside a healthy cardiac muscle cell. More recently, however, indirect experimental evidence has been obtained suggesting the presence of steep concentration gradients near the sarcolemma, particularly during large ion fluxes and possibly enhanced by restricted diffusion in the subsarcolemmal fuzzy space (Leblanc and Hume, 1990; Lederer et al., 1990). This notion was supported by computer models of Ca^{2+} entry and diffusion within the diadic cleft of ventricular myocytes where the local Ca^{2+} concentration was predicted to rise close to millimolar levels (Langer and Peskoff, 1996; Soeller and Cannell, 1997). Considering the conditions in this microenvironment, a major effect of the stationary low-affinity Ca^{2+} binding sites on the phospholipids was anticipated. In our simulations of atrial myocytes without T-tubules and triads, the diffusion barrier arising from the sarcoplasmic reticulum was not implemented as a localized and absolutely impermeable membrane (i.e., a diad). Instead, a subsarcolemmal restricted space was sim-

ulated with the possibility to set (slow down or accelerate) the diffusion in this layer independent of the cytosolic space. This more closely represents the particular cytoarchitecture of atrial myocytes, where peripheral couplings between the sarcolemma and SR have been described. In these regions the diffusion of Ca^{2+} may be more limited and higher Ca^{2+} concentrations may occur, particularly during Ca^{2+} release from the SR (Langer and Peskoff, 1996; Soeller and Cannell, 1997; Peskoff and Langer, 1998; Haddock et al., 1999; MacKenzie et al., 2001; Cordeiro et al., 2001). Our simulations suggest that during Ca^{2+} influx (i.e., without Ca^{2+} release from the SR), the buffering effect of the phospholipids is small, at least in the presence of mobile buffers in the restricted space. These simulations predict significantly elevated Ca^{2+} concentrations in the restricted space only when Ca^{2+} diffusion was slowed down dramatically by eliminating all the mobile Ca^{2+} buffers. Therefore, the phospholipid buffering of Ca^{2+} may be less important in atrial myocytes that lack T-tubules and triads than in ventricular myocytes.

CONCLUSIONS

Taken together, our experimental data and computer simulations imply that in atrial cardiac myocytes lacking T-tubules, Ca^{2+} movement from the cell membrane to the center of the cell relies strongly on the presence of mobile Ca^{2+} buffers. Even at the modest elevations of $[Ca^{2+}]_i$ reached during influx of Ca^{2+}, ATP may act as a significant carrier for Ca^{2+} due to its abundance and despite its low Ca^{2+} affinity. Not considering secondary events, our simulations suggest that the overall effect of kinetically fast soluble Ca^{2+} buffers is at least threefold: 1) mobile Ca^{2+} buffers accelerate the Ca^{2+} movement from the cell periphery to the center; 2) mobile buffers reduce the build-up of large subsarcolemmal concentration gradients during influx of Ca^{2+}; and 3) owing to their sheer buffering capacity, Ca^{2+} buffers tend to reduce the amplitude of Ca^{2+} transients. Ca^{2+} has to diffuse to the center of the atrial cells to activate the contractile proteins located in this space. In atrial myocytes with an intact and functional SR, the Ca^{2+} signal most likely spreads rapidly from the periphery to the center because it is accelerated by a reaction-diffusion wave, driven by Ca^{2+}-induced Ca^{2+} release.

We thank Dr. D. Duridanova for help with atrial cell isolation and D. Lüthi for technical assistance. The authors are grateful to Drs. A. McCulloch and P. Vassilevski for helpful discussions.

This project was supported by the Swiss National Science Foundation with grants to A.M. and E.N. (7BUPJ048575 and 7BUPJ041424).

REFERENCES

Adachi-Akahane, S., L. Cleemann, and M. Morad. 1996. Cross-signaling between L-type Ca^{2+} channels and ryanodine receptors in rat ventricular myocytes. *J. Gen. Physiol.* 108:435–454.

Allbritton, N. L., T. Meyer, and L. Stryer. 1992. Range of messenger action of calcium ion and inositol 1,4,5-triphosphate. *Science.* 258:1812–1815.

Backx, P. H., P. P. de Tombe, J. H. K. Van Deen, B. J. M. Mulder, and H. E. D. J. ter Keurs. 1989. A model of propagating calcium-induced calcium release mediated by calcium diffusion. *J. Gen. Physiol.* 93: 963–977.

Baylor, S. M., and S. Hollingworth. 1998. Model of sarcomeric Ca^{2+} movements, including ATP Ca^{2+} binding and diffusion, during activation of frog skeletal muscle. *J. Gen. Physiol.* 112:297–316.

Berlin, J. R., J. W. M. Bassani, and D. M. Bers. 1994. Intrinsic cytosolic calcium buffering properties of single rat cardiac myocytes. *Biophys. J.* 67:1775–1787.

Bers, D. M. 2001. Excitation-Contraction Coupling and Cardiac Contractile Force. Kluwer Academic Press, Dordrecht, Boston, London.

Burt, J. M., and G. A. Langer. 1983. Ca^{2+} displacement by polymyxin B from sarcolemma isolated by "gas dissection" from cultured neonatal rat myocardial cells. *Biochim. Biophys. Acta.* 729:44–52.

Cannell, M. B., and D. G. Allen. 1984. Model of calcium movements during activation in the sarcomere of frog skeletal muscle. *Biophys. J.* 45:913–925.

Cannell, M. B., J. R. Berlin, and W. J. Lederer. 1987. Effect of membrane potential changes on the calcium transient in single rat cardiac muscle cells. *Science.* 238:1419–1423.

Carafoli, E. 1985. The homeostasis of calcium in heart cells. *J. Mol. Cell. Cardiol.* 17:203–212.

Cheng, H., W. J. Lederer, and M. B. Cannell. 1993. Calcium sparks: elementary events underlying excitation-contraction coupling in heart muscle. *Science.* 262:740–744.

Cheng, H., M. R. Lederer, W. J. Lederer, and M. B. Cannell. 1996. Calcium sparks and $[Ca^{2+}]_i$ waves in cardiac myocytes. *Am. J. Physiol. Cell Physiol.* 39:C148–C159.

Cordeiro, J. M., K. W. Spitzer, W. R. Giles, P. E. Ershler, M. B. Cannell, and J. H. B. Bridge. 2001. Location of the initiation site of calcium transients and sparks in rabbit heart Purkinje cells. *J. Physiol.* 531: 301–314.

Crank, J. 1975. The Mathematics of Diffusion. Oxford University Press, New York.

Dawson, S. P., J. Keizer, and J. E. Pearson. 1999. Fire-diffuse-fire model of dynamics of intracellular calcium waves. *Proc. Natl. Acad. Sci. USA.* 96:6060–6063.

Eberhard, M., and P. Erne. 1989. Kinetics of calcium binding to fluo-3 determined by stopped-flow fluorescence. *Biochem. Biophys. Res. Commun.* 163:309–314.

Egger, M., and E. Niggli. 1999. Regulatory function of Na-Ca exchange in the heart: milestones and outlook. *J. Membr. Biol.* 168:107–130.

Ellis-Davies, G. C. R., J. H. Kaplan, and R. J. Barsotti. 1996. Laser photolysis of caged calcium: rates of calcium release by nitrophenyl-EGTA and DM-nitrophen. *Biophys. J.* 70:1006–1016.

Fabiato, A. 1983. Calcium-induced release of calcium from the cardiac sarcoplasmic reticulum. *Am. J. Physiol. Cell Physiol.* 245:C1–C14.

Fawcett, D. W., and N. S. McNutt. 1969. The ultrastructure of the cat myocardium. I. Ventricular papillary muscle. *J. Cell Biol.* 42:1–45.

Forbes, M. S., and N. Sperelakis. 1982. Bridging junctional processes in coupling of skeletal, cardiac and smooth muscle. *Muscle Nerve.* 5:674–681.

Forbes, M. S., and E. E. Van Niel. 1988. Membrane systems of guinea pig myocardium: ultrastructure and morphometric studies. *Anat. Rec.* 222: 362–379.

Gabso, M., E. Neher, and M. E. Spira. 1997. Low mobility of the Ca^{2+} buffers in axons of cultured *Aplysia* neurons. *Neuron.* 18:473–481.

Gomez, A. M., H. H. Valdivia, H. Cheng, M. R. Lederer, L. F. Santana, M. B. Cannell, S. A. McCune, R. A. Altschuld, and W. J. Lederer. 1997. Defective excitation-contraction coupling in experimental cardiac hypertrophy and heart failure. *Science.* 276:800–806.

Haddock, P. S., W. A. Coetzee, E. Cho, L. Porter, H. Katoh, D. M. Bers, M. S. Jafri, and M. Artman. 1999. Subcellular $[Ca^{2+}]_i$ gradients during excitation-contraction coupling in newborn rabbit ventricular myocytes. *Circ. Res.* 85:415–427.

Harkins, A. B., N. Kurebayashi, and S. M. Baylor. 1993. Resting myoplasmic free calcium in frog skeletal muscle fibers estimated with fluo-3. *Biophys. J.* 65:865–881.

Hüser, J., S. L. Lipsius, and L. A. Blatter. 1996. Calcium gradients during excitation-contraction coupling in cat atrial myocytes. *J. Physiol.* 494.3: 641–651.

Jafri, M. S., and J. Keizer. 1995. On the roles of Ca^{2+} diffusion, Ca^{2+} buffers, and the endoplasmic reticulum in IP_3-induced Ca^{2+} waves. *Biophys. J.* 69:2139–2153.

Jiang, Y., M. G. Klein, and M. F. Schneider. 1999. Numerical simulation of Ca^{2+} "sparks" in skeletal muscle. *Biophys. J.* 77:2333–2357.

Kargacin, G. J., and F. S. Fay. 1991. Ca^{2+} movement in smooth muscle cells studied with one- and two-dimensional diffusion models. *Biophys. J.* 60:1088–1100.

Kargacin, M. E., and G. J. Kargacin. 1997. Predicted changes in concentrations of free and bound ATP and ADP during intracellular Ca^{2+} signaling. *Am. J. Physiol. Cell Physiol.* 273:C1416–C1426.

Keizer, J., and G. D. Smith. 1998. Spark-to-wave transition: saltatory transmission of calcium waves in cardiac myocytes. *Biophys. Chem.* 72:87–100.

Klingauf, J., and E. Neher. 1997. Modeling buffered Ca^{2+} diffusion near the membrane: implications for secretion in neuroendocrine cells. *Biophys. J.* 72:674–690.

Kockskämper, J., and H. G. Glitsch. 1997. Sodium pump of cultured guinea pig atrial myocytes. *Ann. N.Y. Acad. Sci.* 834:354–356.

Kockskämper, J., K. A. Sheehan, D. J. Bare, S. L. Lipsius, G. A. Mignery, and L. A. Blatter. 2001. Activation and propagation of Ca^{2+} release during excitation-contraction coupling in atrial myocytes. *Biophys. J.* 81:2590–2605.

Kushmerick, M. J., and R. J. Podolsky. 1969. Ionic mobility in muscle cells. *Science.* 166:1297–1298.

Langer, G. A., and A. Peskoff. 1996. Calcium concentration and movement in the diadic cleft space of the cardiac ventricular cell. *Biophys. J.* 70:1169–1182.

Langer, G. A., and T. L. Rich. 1986. Augmentation of sarcolemmal Ca by anionic amphiphile: contractile response of three ventricular tissues. *Am. J. Physiol. Heart Circ. Physiol.* 250:H247–H254.

Leblanc, N., and J. R. Hume. 1990. Sodium current-induced release of calcium from cardiac sarcoplasmic reticulum. *Science.* 248:372–376.

Lederer, W. J., E. Niggli, and R. W. Hadley. 1990. Sodium-calcium exchange in excitable cells: fuzzy space. *Science.* 248:283.

Lipp, P., C. Lüscher, and E. Niggli. 1996. Photolysis of caged compounds characterized by ratiometric confocal microscopy: a new approach to homogeneously control and measure the calcium concentration in cardiac myocytes. *Cell Calcium* 19:255–266.

Lipp, P., L. Pott, G. Callewaert, and E. Carmeliet. 1990. Simultaneous recording of indo-1 fluorescence and Na^+/Ca^{2+} exchange current reveals two components of Ca^{2+} release from sarcoplasmic reticulum of cardiac atrial myocytes. *FEBS Lett.* 275:181–184.

MacKenzie, L., M. D. Bootman, M. J. Berridge, and P. Lipp. 2001. Predetermined recruitment of calcium release sites underlies excitation-contraction coupling in rat atrial myocytes. *J. Physiol.* 530:417–429.

Michailova, A., F. DelPrincipe, D. Duridanova., and E. Niggli. 1999. Computer modeling of Ca^{2+} diffusion during Ca^{2+} signaling in atrial cells. *Biophys. J.* 76:459*a*. (Abstr.).

Neher, E., and G. J. Augustine. 1992. Calcium gradients and buffers in bovine chromaffin cells. *J. Physiol.* 450:273–301.

Niggli, E. 1999. Localized intracellular calcium signaling in muscle: calcium sparks and calcium quarks. *Annu. Rev. Physiol.* 61:311–335.

Peskoff, A., and G. A. Langer. 1998. Calcium concentration and movement in the ventricular cardiac cell during an excitation-contraction cycle. *Biophys. J.* 74:153–174.

Post, J. A., and G. A. Langer. 1992. Sarcolemmal calcium binding sites in heart. I. Molecular origin in "gas-dissected" sarcolemma. *J. Membr. Biol.* 129:49–57.

Rios, E., J. J. Ma, and A. Gonzales. 1991. The mechanical hypothesis of excitation-contraction (EC) coupling in skeletal muscle. *J. Muscle Res. Cell Motil.* 12:127–135.

Robertson, S. P., J. D. Johnson, and J. D. Potter. 1981. The time-course of Ca^{2+} exchange with calmodulin, troponin, parvalbumin, and myosin in response to transient increase in Ca^{2+}. *Biophys. J.* 34:559–569.

Schneider, M. F., and W. K. Chandler. 1973. Voltage dependent charge movement of skeletal muscle: a possible step in excitation-contraction coupling. *Nature.* 242:244–246.

Soeller, C., and M. B. Cannell. 1997. Numerical simulation of local calcium movements during L-type calcium channel gating in the cardiac diad. *Biophys. J.* 73:97–111.

Tang, Y., T. Schlumpberger, T. Kim, M. Lueker, and R. S. Zucker. 2000. Effects of mobile buffers on facilitation: experimental and computer studies. *Biophys. J.* 78:2735–2751.

Taylor, S. R., R. Rüdel, and J. R. Blinks. 1975. Calcium transients in amphibian muscle. *Fed. Proc.* 34:1379–1381.

Wagner, J., and J. Keizer. 1994. Effects of rapid buffers on Ca^{2+} diffusion and Ca^{2+} oscillations. *Biophys. J.* 67:447–456.

Zhou, Z., and E. Neher. 1993. Mobile and immobile calcium buffers in bovine adrenal chromaffin cells. *J. Physiol.* 469:245–273.